Numerical Calculation of Current Leads for Fusion Magnets

R. Heller
Institut für Technische Physik
Projekt Kernfusion

Kernforschungszentrum Karlsruhe

NUMERICAL CALCULATION OF CURRENT LEADS FOR FUSION MAGNETS

R. Heller

Abstract

Current leads for high currents up to 50 kA needed for superconducting fusion magnets have to be optimized with respect to heat losses at the cold and warm end to minimize the refrigerator power. Therefore a computer code named CUR-LEAD was written which solves the one-dimensional heat equation for the current lead and the energy balance for the helium coolant simultaneously. This paper describes the physical models and the mathematics used in this program. Special attention has been given to the discussion of the effect of parameter changes on the heat losses and the temperature distribution as well.

Numerische Berechnung von Stromzuführungen für Fusionsmagnete

Zusammenfassung

Stromzuführungen für Ströme bis zu 50 kA, die für supraleitende Fusionsmagnete benötigt werden, müssen im Hinblick auf Verluste sowohl am supraleitenden als auch am normalleitenden Ende ausgelegt werden, um die Kälteleistung zu minimieren. Deshalb wurde das Computerprogramm CURLEAD geschrieben, das die eindimensionale Wärmeleitungsgleichung für die Stromzuführung und die Energiebilanz für die Heliumkühlung simultan löst. Dieser Bericht beschreibt die physikalischen Modelle und die Mathematik, die in das Programm eingeflossen sind. Besonderer Wert wurde auf die Diskussion der Einflüsse von Parameteränderungen auf die Verluste und die Temperaturverteilung entlang des Wärmetauschers gelegt.

Table of Contents

List of Illustrations

List of Tables

Chapter 1. Introduction

Current leads for superconducting magnets which carry high-currents up to 50 kA will play an important role for the design of test facilites for superconducting coils as well as for the coil system of a tokamak reactor like NET [1]. The simple reason is the amount of refrigerator power which cannot be increased above a certain limit. Therefore one has to minimize the heat losses in the whole system e.g. the cryostat or also the current feedthroughs.

The following paper describes the physical model as well as the mathematical approach which both are necessary for the calculation of current leads by means of a computer code.

The paper is subdivided into five parts:

Firstly, the fundamental approach is briefly described which assumes ideal heat transfer from the lead to the coolant and the validity of the Wiedemann-Franz law (neglects the contribution of the electron phonon interaction, e.g. assumes constant Lorentz number).

The disagreement of the calculation of the thermal conductivity k assuming the validity of the Wiedemann-Franz law with the mesurements leads to a modification in the calculation procedure of k. One conclusion is that the calculation of k is simple in case of an oxygen-free-high-conductivity copper (OFHC-Cu), but may be difficult for phosphorized copper (SF-Cu). Therefore the use of experimental data is favoured.

Then the generalisation of the heat conduction problem is discussed, which contains the theoretical description of the heat transfer from the current lead to the coolant, which plays a key role in the physical model. Therefore much space is used for a detailed discussion of heat transfer problems.

In the second part the mathematical methods are briefly described needed for the generation of the computer code. Also the problems concerning transient heat conduction are reflected.

The third part contains the discussion of parameters which are sensitive to geometrical changes during the optimization study e.g. the heat losses at the cold

and warm ends and the temperature distribution along the length of the current lead. In addition the physical aspects of the lead behaviour in case of a losses of coolant are discussed.

The fourth part gives some examples of current leads which has been built in different institutes for different purposes e.g. an 18 kA vapour cooled current lead built for design studies for the proposed Large-Hadron-Collider (LHC) at CERN [2] and a 15 kA current lead built for the TORE SUPRA fusion experiment at CEA [3].

Finally a 23 kA current lead for the POLO experiment now under development at the Institute for Technical Physics [4] has been calculated and optimized for different conditions. Special attention is given to the forced flow cooling mode which will be used for this current lead and is also proposed for the NET project, the design of the cold and warm ends, and to an optimization under different running conditions as well.

Chapter 2. Heat conduction and heat transfer

2.1 The ideal heat transfer: the "Wilson scheme"

In the past the optimization of current leads was done in the following way [5]:

The heat transfer from the current lead to the helium coolant was assumed to be so good, that the coolant could take away all produced heat, i.e. the heat transfer efficiency is equal to one and the temperature difference between the (copper)lead and the helium is very small. In addition the validity of the Wiedemann-Franz law was assumed.

Then the one-dimensional heat equation is simply (see Fig. 1):

$$\frac{d}{dx}(k(T) A \frac{dT}{dx}) - f \dot{m} c_p dT + I^2 \rho(T) \frac{dx}{A} = 0, \qquad (2.1)$$

where
$k(T)$ = thermal conductivity $(\frac{W}{mK})$,
$\rho(T)$ = electrical resistivity (Ωm),
$\dot{m}$ = helium mass flow $(\frac{kg}{s})$,
c_p = helium specific heat at constant pressure $(\frac{J}{kg\,K})$,
f = heat transfer efficiency (in general 0.99),
I = current (A),
A = current lead cross section (m^2),
dx = unit length (m),
dT = temperature difference along dx (K).

The heat equation (2.1) can be analytically solved. By minimizing the solution with respect to the length the interesting result has been got, that a current lead with optimized length has minimum heat losses at the cold *and* at the warm end because the optimized temperature distribution has zero slopes at $x = 0$ *and* $x = L$.

In addition [5] got a more universal result,namely:

$$\frac{L\,I}{A} = const = f(RRR), \qquad (2.2)$$
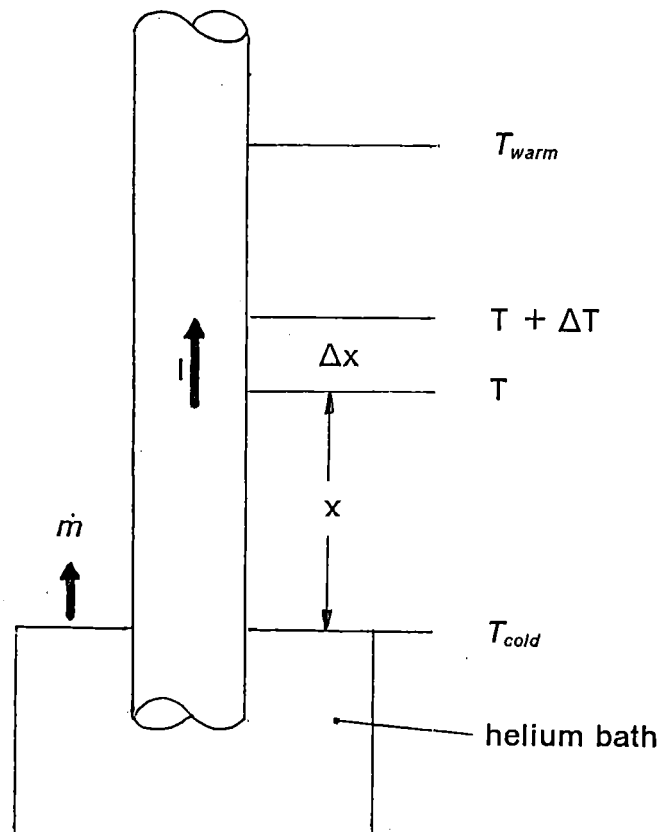
Figure 1.   Schematic view of a current lead

---

i.e. the three parameters I, L, and A are strongly correlated. $\frac{L\,I}{A}$ is called "shape factor".

For example if an oxygen-free copper with high purity (OFHC) with a large residual resistivity ratio (RRR) is used, a value of about $3\ 10^7\ \frac{A}{m}$ has been found for eq. (2.2), i.e. for a given conductor cross section and a given operation current the optimum length can be calculated immediately.

For low conductivity copper [5] stated a shape factor of $3.5\ 10^6\ \frac{A}{m}$. This results in a shorter current lead or a bigger cross section.

In any case there will be an interplay between the generated heat in the lead which decreases with increasing heat conductivity and the heat conduction at the cold end.

Naturally, an appropriate helium mass flow has to be chosen.

In principle the heat flow towards the cold end has to be taken into account, which should be as small as possible. In addition, a current lead made of high conductivity copper will be more sensitive to small changes of the current and/or the mass flow, i.e. the lead will be unstable. Therefore a low-RRR copper is favoured.

As a consequence of the preceeding paragraph the voltage drop along the optimized current lead will be a constant value of 80 mV [5].

2.2 Validity of the Wiedemann-Franz law

Unfortunately the Wiedemann-Franz law is valid only at 4 K and at temperatures above $\sim 40K$. In between the Lorentz number is no more a constant but depends strongly on the temperature. The reason is that the Wiedemann-Franz law doesn't take into account the electron-phonon interaction. In [6] a general parametrization of the thermal conductivity k between 4 K and 40 K is given which results in

$$\frac{1}{k(T)} = \frac{\rho_0}{L_0 T} + a\,T^2, \qquad (2.3a)$$

where

ρ_0 = electrical resistivity at 0 K (Ωm),

$a = 3.35\ 10^{-7}\ \dfrac{m}{W\,K}$,

L_0 = Lorentz number ($= 24.43\ 10^{-9}\ \dfrac{W\Omega}{K}$).

The only free parameter is the electrical resistivity (RRR) at 4 Kelvin.

$$RRR = \frac{\rho(273)}{\rho(4)}, \qquad (2.3b)$$

where

$\rho(273)$ = electrical resistivity at 273 K (Ωm),

$\rho(4)$ = electrical resistivity at 4 K (Ωm).

This modification results in a significant reduction of the thermal conductivity between 4 and 40 K and moreover in a better agreement between the measurements and the calculations. Fig. 2 shows the thermal conductivity as calculated by means of the Wiedemann-Franz law and also by the modified formula given in [6].
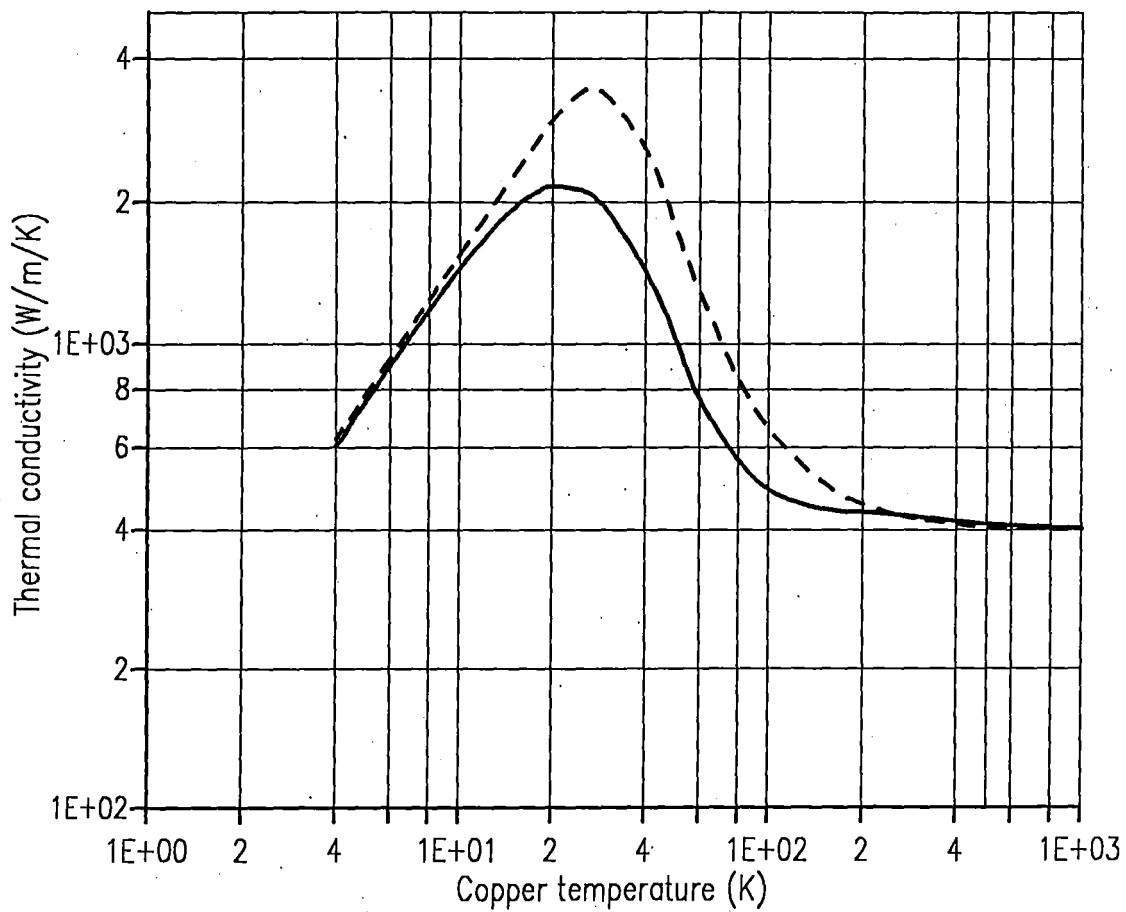
Figure 2. Thermal conductivity, Wiedemann-Franz-law (dashed line) resp. modification by Lock (solid line)

It should be mentioned that sometimes the calculation of the thermal conductivity of low-conductivity copper is troublesome, as for example phosphorized (SF-) copper. Because of its big impurity the theoretical calculation of k as a function of temperature may lead to wrong numbers. Therefore it is more convenient to use measured data which are unfortunately very rare in case of SF-copper [5]. Measurement data are published in [7], whereas an empirical formula is given in [8].

2.3 The real heat transfer in the heat conduction equation

Now eq. (2.1) is discussed. In reality the heat transfer from the current lead to the coolant will depend on the connecting surface. The designer wants to know how big the cooling surface has to be to get a good heat transfer. This question cannot be answered by eq. (2.1). For small surfaces the generated heat cannot be transferred to the cooling gaz, i.e. its temperature will be much lower than that of copper. If the surface is large, one doesn't need a big temperature difference between copper and helium.

In that case eq. (2.1) has to be modified.

$$\frac{d}{dx}(k(T) A \frac{dT}{dx}) - f h(T) P dx(T - T_{He}) + I^2 \rho(T) \frac{dx}{A} = 0, \qquad (2.4a)$$

where in addition

$h(T)$ = heat transfer coefficient ($\frac{W}{m^2 K}$),

P = cooling perimeter (m)

($P dx$ = cooling surface),

f = heat transfer efficiency, temperature independent,

e.g. to account for the "rib efficiency"

T_{He} = temperature of the coolant (K).

The energy balance connects the heat transfer from the lead to the coolant and the mass flow, i.e.

$$\dot{m} c_p dT_{He} - h(T) Pdx(T_{He} - T) = 0. \qquad (2.4b)$$

In the following the properties of $h(T)$ will be decribed in detail [9] .

In general the heat transfer coefficient is a function of the geometry of the heat exchanger and the properties of the coolant, i.e.

$$h(T) = \frac{Nu \lambda}{d_H}, \qquad (2.5)$$

where

Nu = Nusselt number,

λ = helium conductivity ($\frac{W}{m K}$),

d_H = hydraulic diameter (m).

7

The Nusselt number reflects the properties of the coolant and the geometrical boundaries,

$$Nu = f(Re, Pr, d_H),\qquad(2.6)$$

where

Re = Reynolds number,

Pr = Prandtl number.

Different formulas in case of a coolant stream through a pipe or of a stream perpendicular to a series of rods are valid.

On the other hand the Reynolds and Prandtl numbers reflect the helium properties.

$$Re = \frac{u\,\rho_d}{\eta}\,d_H,\qquad(2.7a)$$

$$Pr = \frac{\eta\,c_p}{\lambda},\qquad(2.7b)$$

where

u = flow velocity $(\frac{m}{s})$,

ρ_d = density $(\frac{kg}{m^3})$,

η = dynamic viscosity $(\frac{kg}{ms})$.

The flow velocity u is defined by

$$u = \frac{\dot{m}}{\rho_d\,A_{co}},\qquad(2.8)$$

where

A_{co} = area of the cooling channels (m^2).

In the following the heat transfer coefficient h will be calculated first for a heat flow through a pipe, and then for a heat flow perpendicular to a series of rods.

It should be mentioned that the formulas presented in the following are empiric relations representing a large number of results of experimental data and valid within 10 percent.

2.3.1 Hydrodynamic flow through a pipe

Let us first consider the problem of heat transfer of a pipe which is cooled by a fluid or gaz which flows inside (**parallel-flow model**). For Reynolds numbers higher than 2 800, the following empiric relation has been obtained:

$$Nu = 0.023 \ Re^{0.8} \ Pr^{0.4} \tag{2.9}$$

Eq. (2.9) is called "Dittus-Boelter"-equation and is used in calculations of various current leads [10] - [13] .

Other authors [18] have used a constant Nusselt number because of laminar flow.

$$Nu = 3.8. \tag{2.10a}$$

[9] uses for the calculation of the Nusselt number in case of laminar flow

$$Nu = 0.664 \ \sqrt{Re \ \frac{d_H}{l}} \ Pr^{1/3}, \tag{2.10b}$$

where
l = length of the pipe (m) .

2.3.2 Pressure drop along the current lead

One can also calculate the pressure drop along the heat exchanger.

$$dp = \xi \frac{1}{2} \rho_d \ u^2 \frac{l}{d_H}, \tag{2.11}$$

where
ξ = friction factor.

The friction factor can be calculated by using the Reynolds number Re. For laminar flow (Re < 2800) eq. (2.12a) will be used, whereas for turbulent flow eq. (2.12b) is valid.

$$\xi = \frac{64}{Re}, \tag{2.12a}$$

$$\xi = \frac{0.3164}{Re^{0.25}}. \tag{2.12b}$$

2.3.3 Hydrodynamic flow perpendicular to a series of rods

The formula for calculating the Nusselt number has to be modified in case of a flow perpendicular to a series of rods (**cross-flow model**).

Fig. 3 shows the schematic view of a heat exchanger element made of copper wires forming a net.
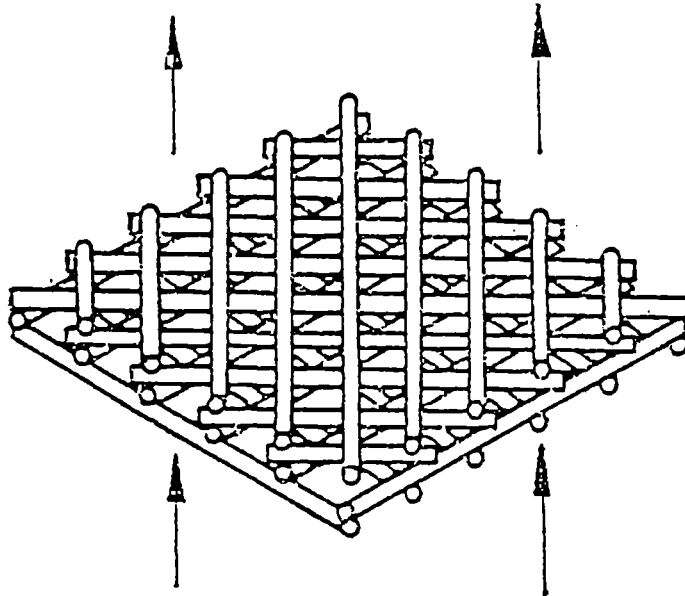
Figure 3.   Schematic view of a heat exchanger element

The reality is simplified in such a way that a net made of copper wires (or also a copper plate with a number of small holes in it) can be handled like a series of rods, see Fig. 4 .

We use the same definitions as in chapter 2.3.1 . For calculating the Nusselt number some correction factors are defined.

$$Nu_{total} = f_\psi N_0,$$
(2.13)

where

Nu_0 = Nusselt number of a single pipe,

f_ψ = ordering factor.

Eq. (2.13) contains the correction factor f_ψ which depends on the specific geometry. One distinguishes between aligned (a) and displaced (b) arrangements (Fig.4).

---

aligned   displaced
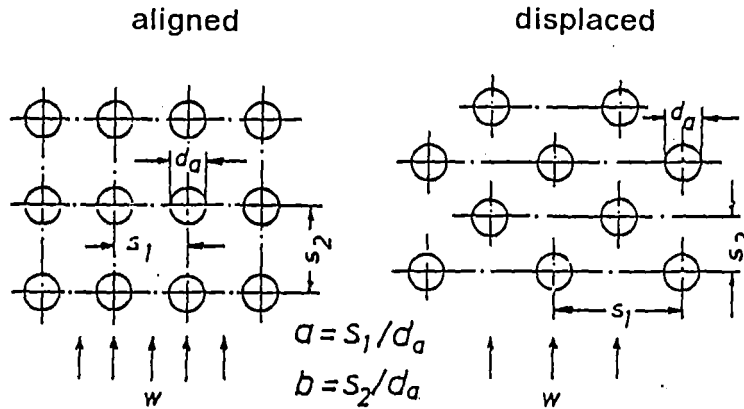
Figure 4. Definition of the geometrical quantities used in the formulas

---

In the following only case (b) will be used, therefore:

$$f_\psi = 1 + (1.87 - \frac{1.7}{b}) \frac{1}{f_1 - 0.4} ,$$
(2.14a)

$$f_1 = \frac{4}{\pi} a \psi.$$
(2.14b)

Using the definitions given in Fig. 4 one gets

$$\psi = 1 - \frac{\pi}{4 a b} .$$
(2.15)

For the Nusselt number of a single rod one combines the equations for laminar and turbulent flow i.e.

$$Nu_0 = \sqrt{0.3 + Nu_{lam}^2 + Nu_{turb}^2} .$$
(2.16)

The laminar and turbulent Nusselt number can be written in the following way (see also eq. 2.10b):

$$Nu_{lam} = 0.664 \sqrt{Re_\psi} \ Pr^{1/3},$$
(2.17a)

$$Nu_{turb} = \frac{0.037\,Re_{\psi}^{0.8}}{1 + 2.443\,Re_{\psi}^{-0.1}(Pr^{2/3} - 1)}, \tag{2.17b}$$

where

Re_{ψ} = corrected Reynolds number.

The heat transfer coefficient h(T) and the modified Reynolds number Re_{ψ} can be written as (see eq. (2.5) resp. (2.8a)):

$$h(T) = \frac{Nu\,\lambda}{d_H}, \tag{2.18}$$

$$Re_{\psi} = \frac{u\,\rho_d}{\psi\,\eta}\,l, \tag{2.19}$$

where

$l = 0.5\,\pi d_a$ = stream length of the single rod = hydraulic diameter (d_a= rod diameter) (m),

u = flow velocity of the coolant before entering of the bundle of rods $(\frac{m}{s})$.

It should be mentioned that in case of a crossing arrangement similar have been obtained. Taken into account that the given formulars are sensitive to 10 - 20 percent there is no need to correct for that purpose.

2.3.4 Pressure drop along the current lead

In case of the described flow perpendicular to rods one can also calculate the pressure drop along the heat exchanger.

$$\frac{1}{N}\frac{dp}{dx} = \xi\frac{1}{2}\,\rho_d\,u_m^2\,\frac{1}{d'}, \tag{2.20}$$

where

N = number of rod rows in flow direction,

ξ = friction factor,

$$u_m = \frac{u}{1 - \dfrac{\pi}{4\,a}},$$

$$d' = (\frac{4\,a}{\pi} - 1)\,l\,.$$

The friction factor can be calculated by using the Reynolds number Re.

$$\xi = 2 \left[\frac{64}{Re_\psi} + \frac{2}{Re_\psi^{0.18}} \right].$$

(2.21)

Eq. (2.21) is valid both for laminar and turbulent flow.

Chapter 3. Realization of the 1-D heat conduction problem by a finite-difference equation

3.1 Application of finite-difference equations

Consider the problem of the heat conduction in one dimension. In case of a steady state problem the temperature T satisfies the simplest differential equation of elliptic type

$$k\frac{d^2T}{dx^2} + H = 0, \tag{3.1}$$

where k is the thermal conductivity and H is the internal heat generation rate per unit volume. This equation can be represented by using the simplest finite difference formula for second derivatives [14], [15] :

$$(\Delta x)^2 \left(\frac{d^2T}{dx^2}\right)_{x=x_0} = T(x_0 + \Delta x) - 2\,T(x_0) + T(x_0 - \Delta x). \tag{3.2}$$

This results in the following finite difference equation at the point $x = x_0$:

$$k[T(x + \Delta x) + T(x - \Delta x) - 2\,T(x)] + \Delta x^2\, H(x) = 0. \tag{3.3}$$

Of course this equation can also be obtained directly from the energy balance for a small interval Δx with centre x. The energy balance states that for this problem

Net rate at which heat is absorbed + Rate of internal heat generation = 0

The usual boundary conditions associated with the elliptic equations are of two kinds, either
(i) specified values at T, or
(ii) a condition on its normal gradient of the form

$$k\frac{dT}{dn} = -h(T - T_A), \tag{3.4}$$

representing a linear heat transfer by convection into an ambient node of temperature T_A .

In Fig. 5 top some internal nodes for the current leads and the helium are shown, whereas in Fig. 5 bottom boundary nodes are plotted. The energy balances are also shown.
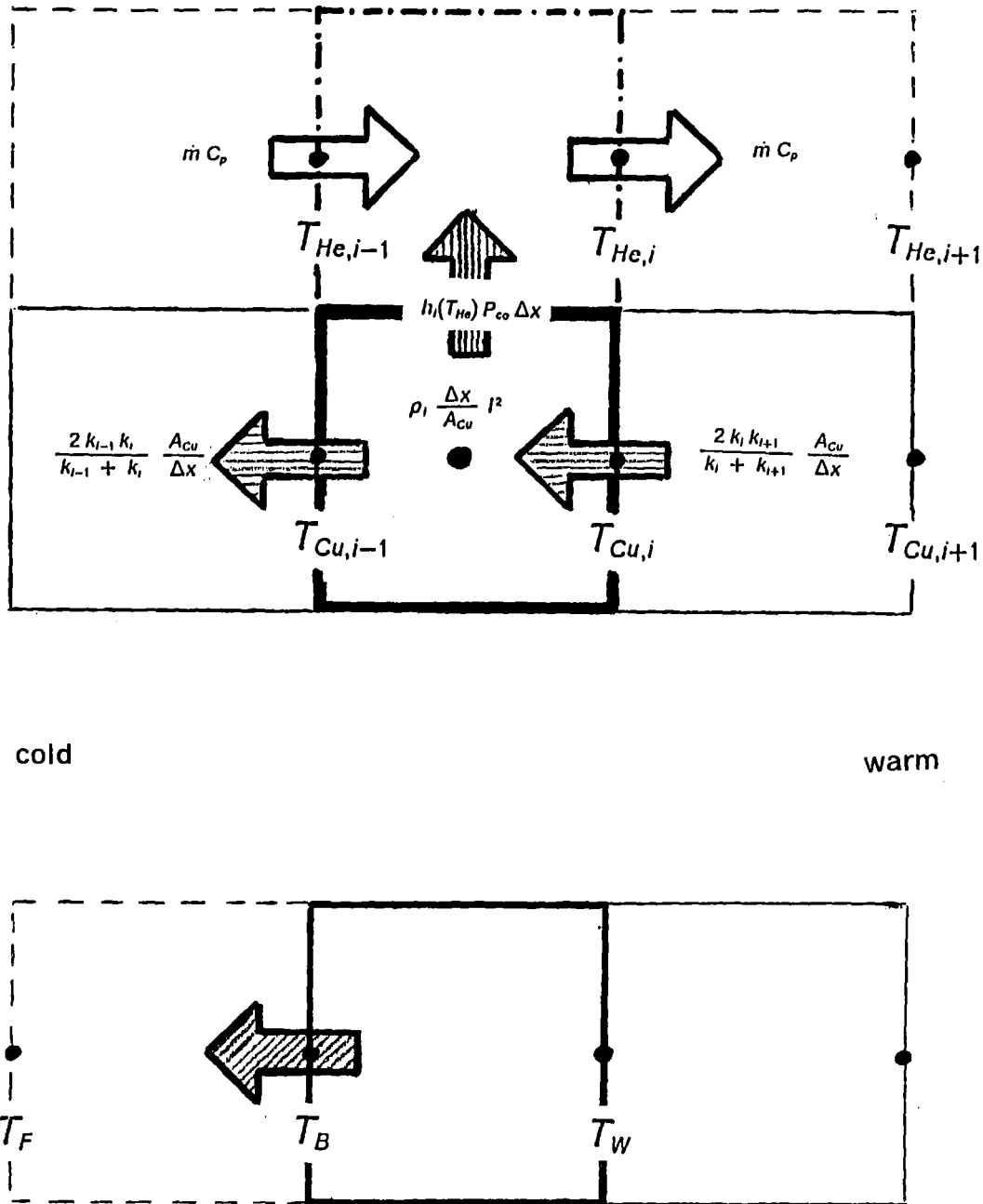
Figure 5. Scheme of the discretization elements:
top: internal nodes of copper and helium
bottom: boundary nodes of copper

Finite difference simulation of steady-state and transient heat conduction by implicit schemes leads to systems of many algebraic equations which must be solved simultaneously. They have a unique solution, but in reality it may be difficlut to solve these equations with considerable accuracy, compatibility and convergency. Methods of solution can be classified as direct or iterative.

Direct methods obtain the solution directly in a finite number of operations. For linear cases the problem is then finished, but for quasi-linear problems (e.g. the material constants are temperature dependent) the process must be repeated with updated coefficients evaluated based on the currently computed temperature.

Direct methods are invariably used in case of on spare systems of equations where the occurence of non-zero elements follows a particular simple pattern, like a tridiagonal system where the Gauss elimination direct process takes a particularly simple form known as tridiagonal matrix algorithm (TDMA). Such problems, in which each equation contains exactly three unknowns, except the first and last equations which contain two unknowns, result in so-called tridiagonal equations sets, the matrix form of which would comprise a tridiagonal band of coefficients, and these are better solved by direct methods. Such equation sets occur in:

- 1-D steady state problems and in
- the solution of transient problems by implicit methods.

3.2 The tridiagonal algorithm

The discretization of eq. (3.3) is used for each node (see also Fig. 5 top and Fig. 5 bottom). The following sets of n linear equations for the n unknowns have to be solved:

$$
\begin{aligned}
a_{11}T_1 + a_{12}T_2 + \ldots + a_{1n}T_n &= b_1 \\
a_{21}T_1 + a_{22}T_2 + \ldots + a_{2n}T_n &= b_2 \\
\ldots &= \ldots \\
a_{n1}T_1 + a_{n2}T_2 + \ldots + a_{nn}T_n &= b_n
\end{aligned}
\tag{3.5}
$$

where e.g. for the i-th node

$$
a_{ii-1} = -\frac{2\,k_{i-1}\,k_i}{k_{i-1} + k_i}
$$

$$a_{ii} = \frac{2 k_{i-1} k_i}{k_{i-1} + k_i} + \frac{2 k_i k_{i+1}}{k_i + k_{i+1}} + h_i(T) P \Delta x \qquad (3.6)$$

$$a_{ii+1} = -\frac{2 k_i k_{i+1}}{k_i + k_{i+1}}$$

$$b_i = I^2 \rho_i(T) \frac{\Delta x}{A_{Cu}} + h_i(T) P \Delta x T_{He}$$

With direct solution methods, a finite number of operations yields the solution but there is a build-up of round-off errors which can lead to irregular solutions.

Elementary elimination may be used to solve an equation like eq. (3.5). This leads to the modified sets of equations:

$$a_{11}T_1 + a_{12}T_2 + \ldots + a_{1n}T_n = b_1$$
$$a'_{22}T_2 + \ldots + a'_{2n}T_n = b'_2 \qquad (3.7)$$
$$\ldots = \ldots$$
$$a'_{nn}T_n = b'_n$$

where primes denote the modified coefficients, e.g. for the i-th equation

$$a'_{ii} = a_{ii} - \frac{a_{ii-1}}{a'_{i-1i-1}} a'_{i-1i}, i = 2,3,\ldots,n$$

$$b'_i = b_i - \frac{a_{ii-1}}{a'_{i-1i-1}} b'_{i-1}, i = 2,3,\ldots,n \qquad (3.8)$$

It can be shown that this elimination process is always possible. If zero coefficients occur for example in the rth equation, some ordering in equations r, r+1,...,n can obtain a non-zero coefficient of T_r in the rth equation, and the process can continue.

This is always possible, provided the given eqs. (3.5) are linearly independent, and therefore the corresponding matrix A can be inverted.

Starting from eq. (3.7) the last unknown can be found:

$$T_n = \frac{b'_n}{a'_{nn}}, \qquad (3.9a)$$

and the rest follows by back-substitution via

$$T_r = \frac{b'_r - \displaystyle\sum_{i=r+1}^{n} a'_{ri}T_i}{a'_{rr}}, \qquad (3.9b)$$

where $r = n-1, n-2, \ldots, 1$.

3.3 Iterative solution methods

As already mentioned above, iterative methods are needed in case of temperature dependent coefficients in eq. (3.5) resp. (3.7). There is no build-up of rounding errors as the solution is generated, but in order to guarantee an adequate solution a dominant diagonal coefficient is required. That is, in the previous equation set:

- the diagonal coefficient a_{ii} in the ith equation (for each i in turn, $1 < i < n$) must be at least (in absolute magnitude) as large as the sum of the absolute magnitude of all other coefficients on the left of the ith equation, i.e.

$$|a_{ii}| \geq |a_{i,1}| + \ldots + |a_{i,i-1}| + |a_{i,i+1}| + \ldots + |a_{in}| \qquad (3.10a)$$

for each i $(1 \leq i \leq n)$,

- for at least one of the equations the diagonal coefficient must be strictly larger than the others, i.e.

$$|a_{ii}| > |a_{i,1}| + \ldots + |a_{i,i-1}| + |a_{i,i+1}| + \ldots + |a_{in}| \qquad (3.10b)$$

for at least one i $(1 \leq i \leq n)$.

These requirements are usually no problem in practice, because in case of steady-state elliptic problems equation sets are automatically obtained which may be arranged in dominant diagonal form. The method generally starts from an approximate solution and repeatedly updates the T values many times until the updated results are of little difference to the former T values. Often the Tschebychev norm is used as a convergence criterion:

$$\max_i \left| \frac{T'_i - T_i}{T'_i} \right| < TOL. \qquad (3.11)$$

18

where

T_i = temperature of i-th node of current iteration,

T'_i = temperature of i-th node of last iteration,

TOL = tolerancy.

The problem concerning the convergency will be discussed later on.

3.4 Boundary conditions

The boundary nodes and the incorporation of boundary conditions appropriate to the problem have been slightly mentioned. Consider a problem which has a grid system covering the solution domain with boundaries coinciding with mesh lines. In order to be soluble a finite difference equation (FDE) must be provided for each one of the entire set of node points, which in general consists of all internal points and all boundary points. The FDE for each internal point can be deduced from the preceeding paragraphs; the objective here is to find an equation for each boundary point.

In heat transfer problems two cases often occur for each boundary point:

- Boundary surface temperature is known (Dirichlet condition), in which case

$$T_B = T_G,\tag{3.12}$$

  where T_G is the known temperature given in the problem specification.
- Boundary surface temperature is not known (Neumann condition), in which case the additional problem specification is in the form of knowledge about the outward normal gradient of temperature dT/dn. This may be:

$$\frac{dT}{dn} = K = -\frac{h}{k}(T_B - T_A),\tag{3.13}$$

  where h is the surface heat transfer coefficient, k is the thermal conductivity, and T_B and T_A are boundary and ambient temperatures, respectively.

The problem of incorporation of eqs. (3.12) and (3.13) into the FDEs for the boundary nodes will be discussed briefly. Eq. (3.12) in fact presents no new problem, since if the boundary temperatures are known, they can be inserted easily into the

relevant FDEs. The Neumann boundary condition will be considered separately. The FDE can be derived by two methods, the direct replacement of the partial differential equation and the energy balance method. But only the latter one will be used and only the final result will be shown here, while a more detailed description is given in [14].

If the temperature gradient at the boundaries implies the knowledge of the heat loss per surface area, then (see Fig. 5 bottom).

$$T_F = T_W - 2\frac{\Delta x}{k} Q_{heat},$$ (3.14)

where

T_F = fictitious temperature node outside,

T_W = first interior node temperature.

3.5 Stability and convergence

There are two types of errors. The first one is called truncation error and is due to computing with derivatives replaced by finite differences. This depends on the initial given temperature distribution, the boundary conditions, the choice of finite difference scheme, and (for transient problems) the choice of the Fourier number Fo used in the computation. The second type of error are numerical: round-off errors which are caused by the finite significant figure restriction used in any calculation, and errors which - for a given space-time grid associated with Fo - are inherent in certain finite difference schemes being unstable with respect to the propagation and growth of oscillatory values as the computed solution. Special problems concerning the stability and accuracy of transient heat conduction calculations will be discussed in the following.

In chapter 4 the convergency and accuracy problems related with the definition of the one-dimensional grid (the step size) will be described in more detail, because these studies are crucial points for the interpretation of the computational results.

3.6 Transient heat conduction - the Fourier number

Consider the transient behaviour of the one-dimensional heat equation. In that case the difference between the heat produced and dissipated is non-zero and results in a temperature change at any node with time. The associated parabolic equation is

$$\rho C_p \frac{\partial T}{\partial t} = k \frac{\partial^2 T}{\partial x^2} + H, \tag{3.15}$$

where ρ is the density and C_p is the specific heat at constant pressure of the material.

Of course this equation can also be obtained directly from the energy balance. When transient conditions are valid, the temperature of the substances at a given point will be changeing with time. In mathematical terms:

$$\text{Net rate of heat flow} = mC_p \frac{\partial T}{\partial t},$$

where m is the mass of the substance.

The specific heat is a measure of capacity to store heat wheras thermal conductivity indicates the ability of a material to transfer heat. The term 'thermal diffusivity' has been evolved to partially quantify the rate of response:

$$\text{Thermal diffusivity} \propto a = \frac{k}{\rho C_p} \ (m^2/s), \tag{3.16}$$

A dimensionless quantity, called a Fourier number Fo, has been defined to assist in the representation of transient heat flow calculations:

$$Fo = \frac{k\Delta t}{\rho C_p (\Delta x)^2} = \frac{\text{Rate of conduction of heat}}{\text{Rate of storage of heat}}, \tag{3.17}$$

The Fourier number gives an indication of the speed at which a body will respond to a temperature change. Low values of Fo imply the requirement of a long time period to heat or to cool the body, and vice versa.

To translate the transient term into the FDE, the forward-difference representation has to be used which involes $T(t + \Delta t)$ and $T(t)$ at the point P only. This results in the following finite difference equation:

$$T(x + \Delta x, t) + T(x - \Delta x, t) - (2 - \frac{1}{Fo})T(x,t) + \Delta^2 H(x) = \frac{1}{Fo} T(x, t + \Delta t) \quad (3.18)$$

There are considerations with regard to stability, accuracy and convergence of this formula which limit the maximum value of Δt for a given Δx .

Looking on the coefficient in front of $T(x,t)$, it is recognized that the thermodynamic principles are only non-violated if this coefficient will be positive (otherwise the new temperature at time $t + \Delta t$ would be the larger the smaller the old temperature at time t is). This turns out to be in fact a sufficient condition for the stability of explicit FDEs:

$$Fo \leq \frac{1}{2} \quad (3.19a)$$

for the interior nodes, and

$$Fo \leq \frac{1}{2(1 + Bi)} \quad (3.19b)$$

for the boundary nodes, where

$$Bi = \frac{h\Delta x}{k} \quad (3.20)$$

is called the Biot number and measures the amount of surface conductance compared to the thermal conductivity of the solid.

Combining eqs. (3.19a) and (3.19b) one finds

$$\Delta t = \frac{\Delta x^2}{a} \leq \frac{\Delta x^2}{2a(1 + Bi)} , \quad (3.21)$$

Thus if Bi is large, Δt may have to be taken unnecessarily small only for stability reasons, resulting in a substantial increase in computer time.

Fortunately the grid interval Δx will be relatively small in most of our cases, and therefore the Biot number will be small too (small compared to one).

3.7 Choice of the Runge-Kutta method

In the literature another numerical method exists for solving differential equations of n-th order by reducing the problem to n equations of 1st order: the Runge-Kutta method.

The advantage of this method is the amount of computer time which is much less than in case of Gauss elimination, because it's a direct method which starts from a given temperature with a given slope and calculates step by step the next temperature node up to the upper end.

The disadvantage is that there is no possibility to manipulate the heat flux at the warm end terminal. If the current lead is lengthened the upper temperature arises rapidly due to the fact, that the heat conduction stays constant with temperature whereas the heat production increases, and therefore the heat flux increases, too.

Of course, the results obtained with both methods are the same for an optimized current lead, as will be seen in the next chapter.

Chapter 4. Calculation of characteristics of current leads by means of the computer code CURLEAD

4.1 General remarks

A detailed description of the computer code CURLEAD, which has been developed to study and to optimize a high power current lead with respect to heat losses and/or stability, will be given in [16]. Here only some remarks are adopted while a flow chart of the code is presented in the appendix.

CURLEAD offers the possiblity to choose between two different algorithms described in chapter 3, as it is the tridiagonal matrix algorithm (TDMA) and the Runge-Kutta method. Therefore if the whole lead has to be modelled including the cold and/or the warm end terminal, it is recommended to use the time consuming but more realistic TDMA algorithm which offers the possibility to choose between the Dirichlet or the Neumann boundary conditions. Most of the results presented in this report has been got by the TDMA combined with the Dirichlet condition at both ends.

In case of a transient problem, the use of the Runge-Kutta method is excluded.

CURLEAD offers also the possibility to change the geometry of the lead along the length at least 19 times, e.g. copper cross section, cooling perimeter, helium mass flow, and the cooling flow type, as described in chapter 2 in detail. In addition to this there is the possibility to use a currentless piece as a part of the lead, e.g. the heat production can be "switched off", and only the heat conduction is valid. The technical realization is the use of a superconducter in parallel to the copper of the current lead. This technique will be described in chapter 6.

The helium properties namely thermal conductivity λ, density ρ_d, viscosity η, and specific heat c_p are taken from the program package HEPROP [17] which is used also in CURLEAD. This has the advantage that the program allows the user to vary the inlet temperature and pressure. The disadvantage is that the procedure is very time consuming, because the calculation and interpolation for getting λ, ρ_d, η, and c_p has to be done several ten thousand times. The ratio between the CPU-time needed for a program with and without the HEPROP routines is about 5.

In the following, the free parameters in the heat conduction equation are discussed. The effect of parameter changes on the temperature distribution and on the heat losses are presented in detail. At the end of this chapter some attention is given to accuracy and stability problems.

4.2 Free parameters for the heat conduction problem

In Tab. 1 the physical parameters are summarized, which influence the optimization of a current lead (beside the material properties).

Parameters	Code name	Unit	Description
I	CURR	A	current in the current lead
L	XLEN	m	length of the current lead
A_{Cu}	ACCU	m^2	current lead cross section
P_{co}	PERI	m	cooling perimeter
A_{co}	AERHE	m^2	helium flow cross section
$\dot{m}$	FHE	$\frac{g}{s}$	helium mass flow
f	XEFF		heat transfer efficiency
RRR	RRR		residual resistivity ratio
tolerancy	TOL		relative temperature change

Table 1. **Description of parameters which influence the current lead optimization**

Designing a powerful current lead means the optimization by fixing some parameters. The optimization depends on

- running conditions, e.g. kind of current mode,
- boundary conditions of the construction,
- heat losses at the cold end,
- heat losses at the warm end, e.g. frozen if no current, etc.

To give an example, the designer wants to know the amount of cooling surface needed to transfer the produced and conducted heat to the coolant. In general small temperature differences and therefore big cooling surfaces (or cooling perimeters) are favoured.

In the following variables are discussed which are sensitive to parameter changes. In principle the most sensitive parameter will be the helium mass flow. In bath cooled current leads, the heat loss at the cold end directly evaporates helium out of the bath, the latent heat is about 20.9 J/g at 1 bar and 4.2 K. An optimized current lead will produce exactly the amount of helium gaz which is needed for cooling up to 300 K (selfcooling condition). But for forced flow cooled current leads this argument is no more valid, i.e. the mass flow can be independently adjusted from the cold end heat losses. But in any case they have to be minimized because they have to be removed. In chapter 5 and 6 some examples for current leads will be discussed.

4.3 Effect of parameter changes on the temperature profile and on the heat losses

In this chapter the effect of parameter changes will be discussed by using a low conductivity copper current lead. The parameters for this current lead are presented in [5], except the length. Because of the uncertainty of the SF-copper properties of this current lead, a similar distribution of p and k has been used [7], and the according length is somewhat different. Fig. 6 contains the electrical resistivity and the thermal conductivity of the used SF-copper, and for comparison the corresponding distributions for OFHC-copper are also shown. Tab. 2 contains the design parameters and Fig. 7 shows the temperature distribution along the lead.
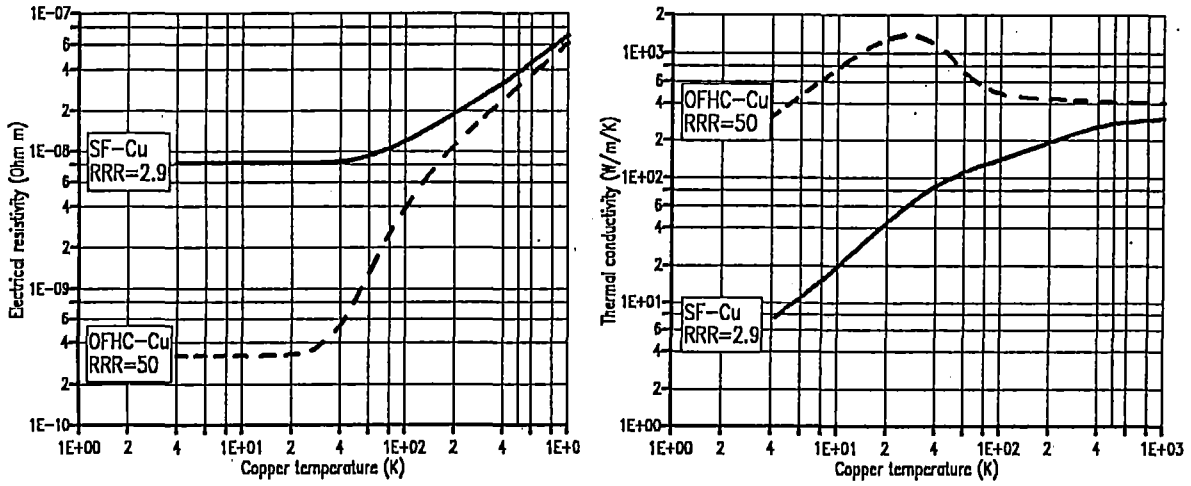
Figure 6. **Electrical resistivity resp. thermal conductivity of SF- and OFHC-copper:** SF-copper - solid line, OFHC-copper - dashed line
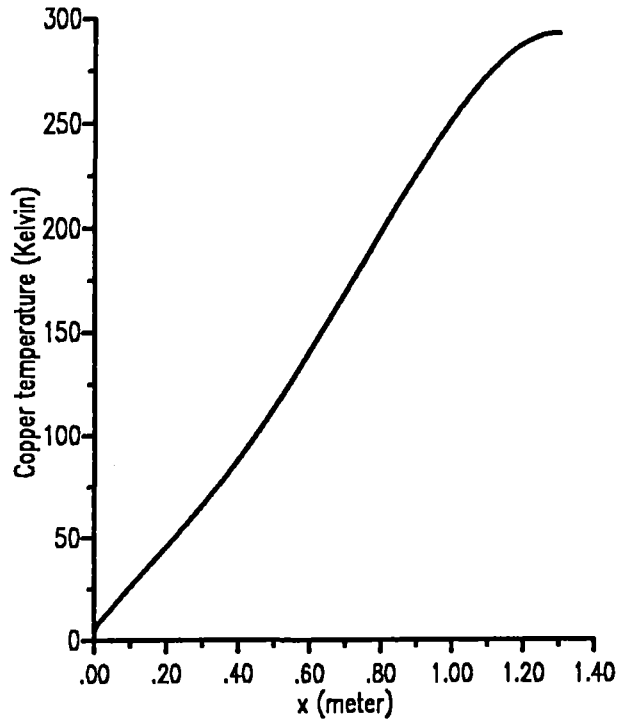
Figure 7. **Temperature distribution of an optimized current lead**

Parameters	Unit	Value
I	A	2000
L	m	1.30
A_{Cu}	m^2	$5.7\ 10^{-4}$
P_{co}	m	1.140
A_{co}	m^2	$2.85\ 10^{-4}$
$\dot{m}$	$\dfrac{g}{s}$	0.10
f		0.5
RRR		2.9
$\dfrac{L\,I}{A_{Cu}}$	$\dfrac{A}{m}$	$4.5\ 10^6$
tolerancy		10^{-5}

Table 2.   Design parameters of a low conductivity copper current lead

Tab. 3 gives the summary of results of the effect of parameter changes discussed in this chapter.

As already mentioned the most sensitive parameter is the helium mass flow. In Fig. 8 the temperature distribution along the current lead is shown for at least three mass flow rates, the nominal one, the 90 percent, and the 110 percent ones. Naturally these are the results of a steady-state problem, i.e. there is no quantitative information about the time after these distributions are obtained. In general several minutes are needed to reach it. At the end of this paragraph quantitative results are shown for the transient case.

Fig. 9 shows the effect of different copper resistivities on the temperature distribution. Three RRR values are chosen, e.g. the nominal one (2.9), then 7.5, and 50. It is clearly seen, that a high conductivity- (or a low resistivity-) copper results in a significantly different shape of the distribution. Compared to the other two, the temperature stays relatively low along the lead over a big fraction of the length,

but at the end, the slope is very high. The reasons are low joule losses at the cold end and relatively high thermal conductivity in a temperature range from 20 K to 200 K (Fig. 6).

The different shapes of the temperature distributions of a low RRR- and a high RRR-copper lead are correlated to the stability of the lead against fluctuations, for example of the current. This will be shown in Fig. 10, where the effect of current changes is plotted for low conductivity copper. The temperature distributions are presented for I/I_{opt} = 1.0, 0.8, and 1.2. Of course the helium mass flow was scaled by the same ratio. If the current would be increased too far above its optimum value, the lead may burn-out. For RRR = 2.9, the maximum temperature of about 500 K has been obtained for I/I_{opt} = 1.6. By using an RRR of 50, the melting point of solder (ca. 450 K) will be reached already for I/I_{opt} = 1.05. For these calculations it was assumed that it is possible to keep the warm end temperature to 300 K. The conclusion is that high conductivity copper can be used for a smaller current region than the low conductivity one.

In Fig. 11 the temperature distributions for several cooling perimeters are plotted for the design value (1.14 m), for a two times larger one (2.28 m), for a 50 percent, and for a 10 percent one. The distribution for the largest value of P_{co} is not well distinguished from that of the designed perimeter, only if the bottom part of the lead is shown, a difference can be recognized (see Fig. 12 top). Fig. 12 bottom shows the temperature difference between the current lead and the helium coolant as a function of the lateral distance x. As already mentioned in chapter 2, the decrease of the cooling perimeter will lead to an increase of the temperature difference $T_{Cu} - T_{He}$. For small perimeter values the temperature in the lead is much higher, because the generated (and conducted) heat cannot be transferred to the cooling medium. This is specifically important at the cold end, whereas in the warmer parts of the lead the characteristics doesn't change. It can also be seen that an increase of the cooling perimeter above 1.14 m will not lead to a significant better heat transfer because it is already possible to transfer all excess heat to the coolant. Fig. 13 shows the heat transfer coefficient as a function of the longitudinal position x. Generally spoken the change of the cooling perimeter at constant cooling channel cross section leads to a change of the hydraulic diameter d_H and therefore to a change of h(T) (see eq. (2.18)).

Fig. 14 shows the temperature distributions at the cold end calculated for different heat transfer efficiencies, i.e. 0.5, 0.98, and 0.2, which doesn't show significant differences for f = 0.98 and f = 0.5. Looking to the cold end losses for these effi-

ciencies, a difference of only 20 percent is observed between f=0.98 and f=0.5, whereas the losses are twice as high in case of f=0.2.

The conclusion is that it is very important to have a good heat transfer at the cold end.

I	$\dot{m}$	RRR	P_{co}	f	Q_{bot}	Q_{top}	ΔU	h_{top}
[kA]	$[\frac{g}{s}]$		[m]		[W]	[W]	[mV]	$[\frac{W}{m^2K}]$
2	0.10	2.9	1.140	0.5	-2.08	-0.46	77.54	583
2	0.09	2.9	1.140	0.5	-3.52	-29.78	86.25	587
2	0.11	2.9	1.140	0.5	-1.56.	25.21	71.16	580
2	0.10	7.5	1.140	0.5	-17.01	86.73	40.05	578
2	0.10	50.0	1.140	0.5	-39.14	148.54	19.37	574
2	0.10	2.9	4.560	0.5	-1.06	5.71	76.32	2330
2	0.10	2.9	2.280	0.5	-1.36	0.43	77.45	1166
2	0.10	2.9	0.570	0.5	-3.99	2.89	76.71	291
2	0.10	2.9	0.114	0.5	-34.78	-3.44	90.74	56
2.4	0.12	2.9	1.140	0.5	-2.90	-62.53	105.40	591
1.6	0.08	2.9	1.140	0.5	-1.47	30.66	56.98	579
2	0.10	2.9	1.140	0.98	-1.64	-0.20	77.54	583
2	0.10	2.9	1.140	0.2	-3.13	1.63	77.0	583

Table 3.   Summary of results of the effect of parameter changes
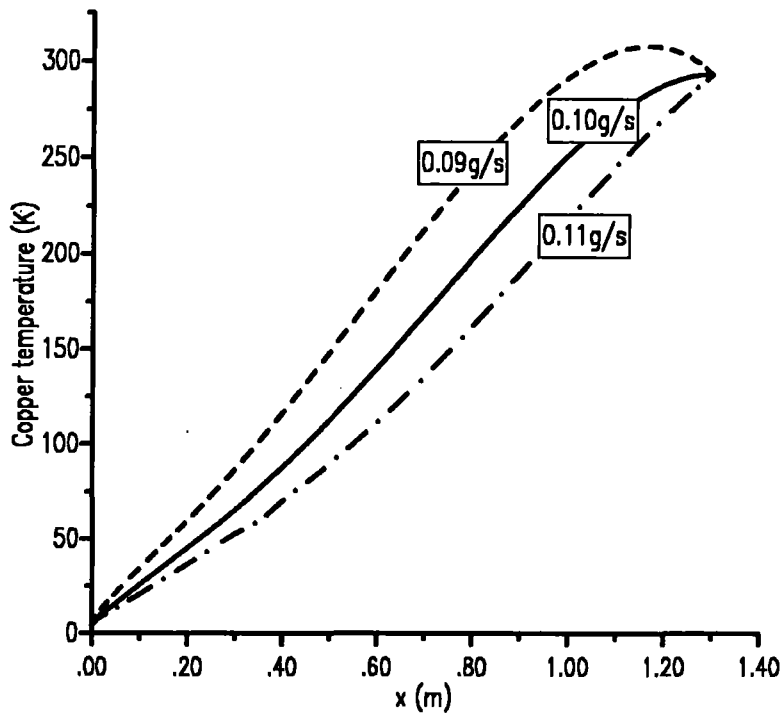
Figure 8. **Different helium mass flow rates** $\dot{m}$: Temperature distribution of an optimized current lead
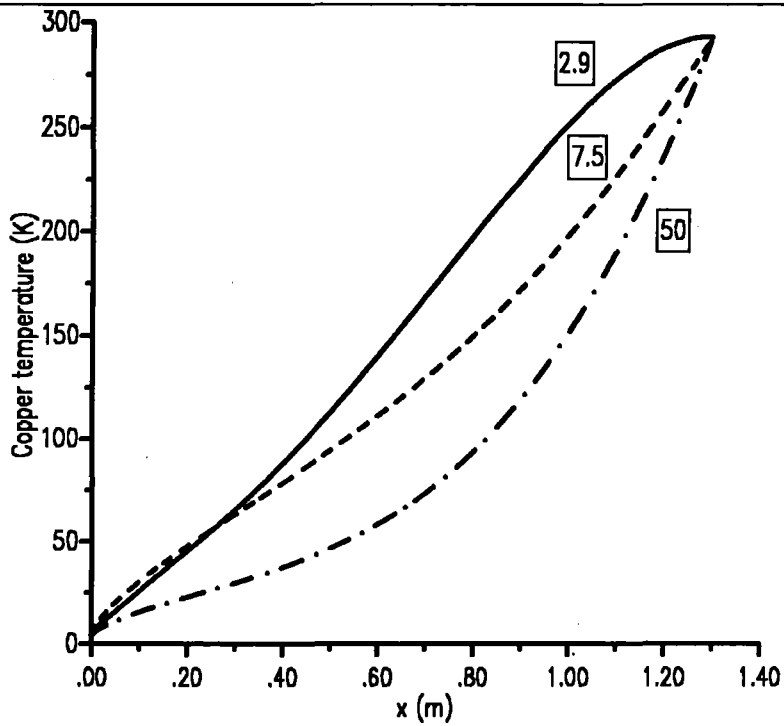
Figure 9. **Different residual resistivity ratios RRR:** Temperature distribution of an optimized current lead
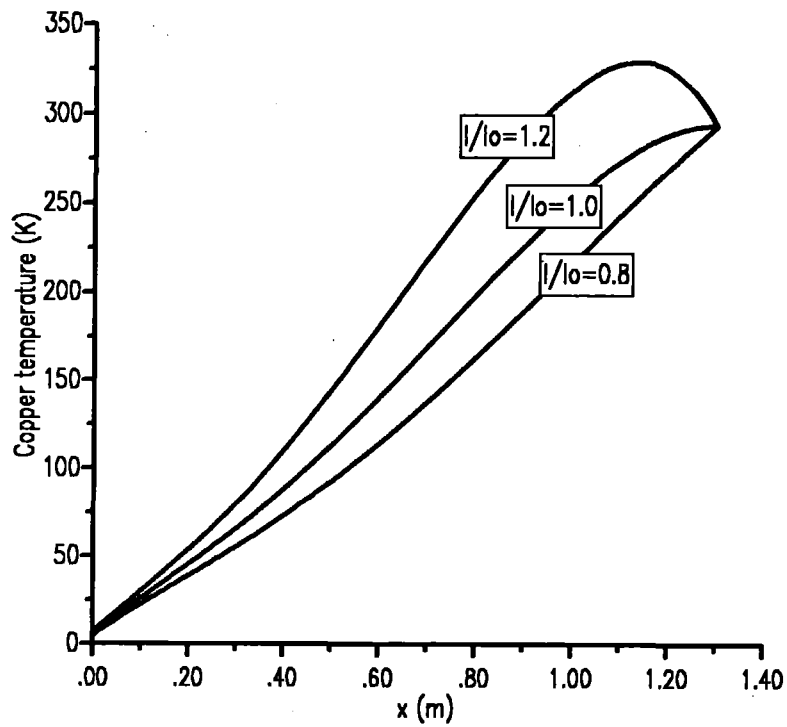
Figure 10. Different currents I: Temperature distribution of an optimized current lead
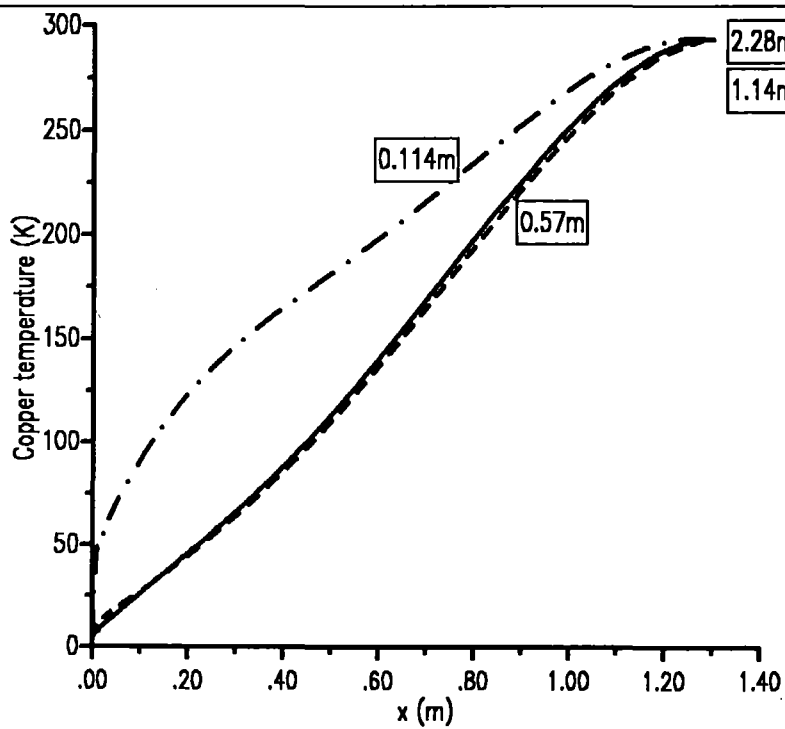
Figure 11. Different cooling perimeters P_{co}**:** Temperature distribution of an optimized current lead
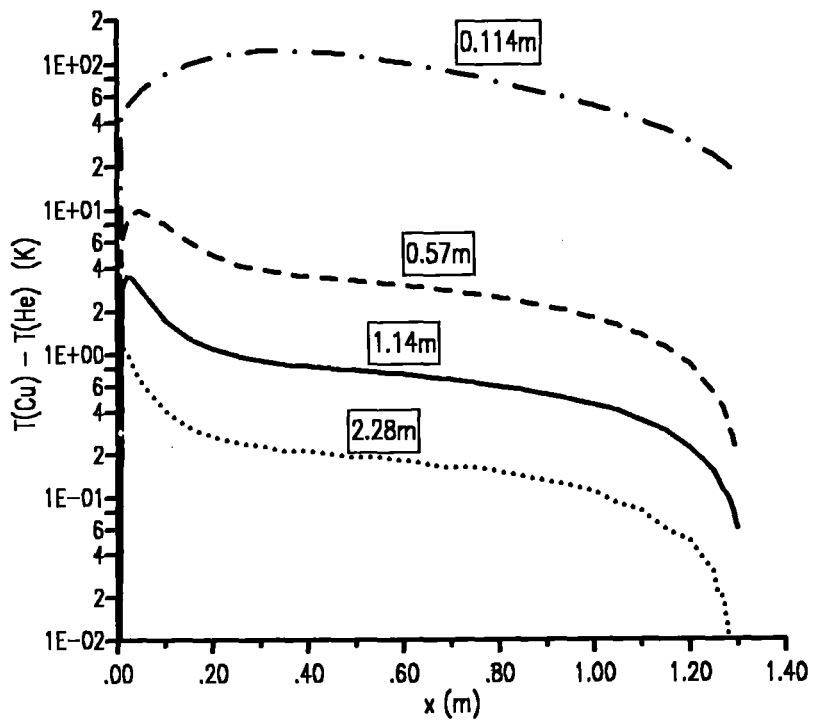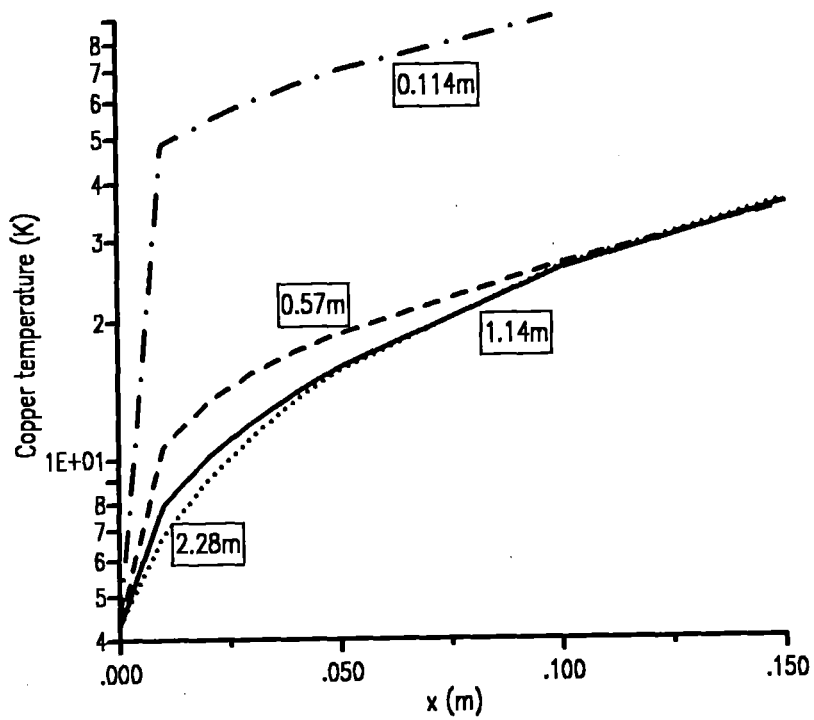
Figure 12. Temperature distribution for different cooling perimeters P_{co}:

top: bottom end of the current lead

bottom: temperature difference between copper and helium
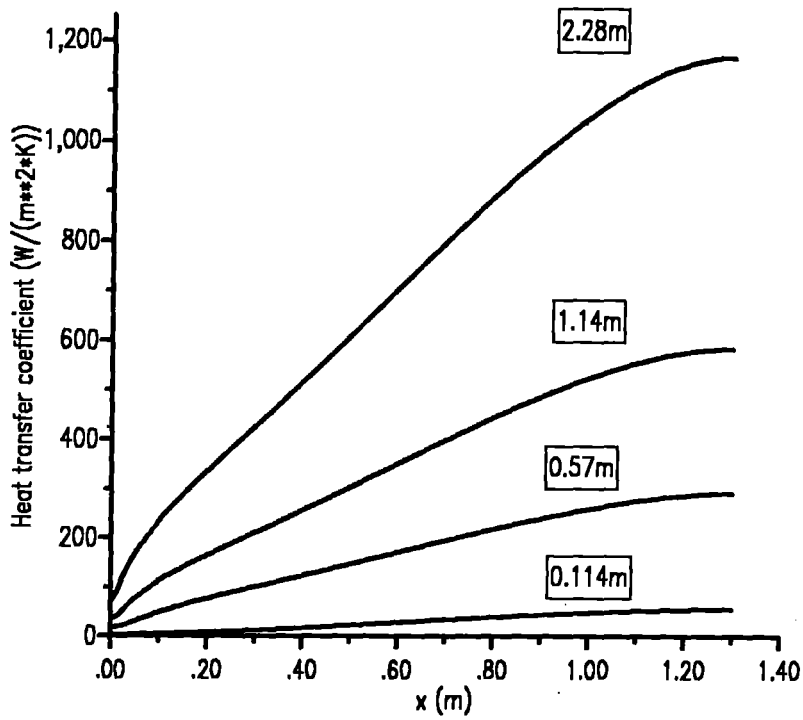
Figure 13. Different cooling perimeters P_{co}: Heat transfer coefficient
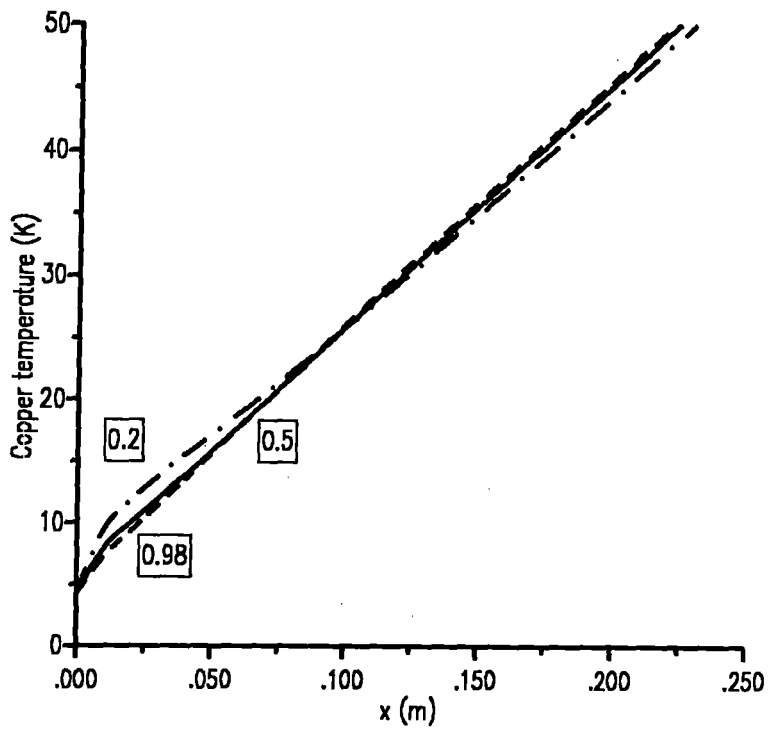
Figure 14. Different heat transfer efficiencies f: Temperature distribution of an optimized current lead

4.4 Transient behaviour

Now the transient case will be discussed in case of a loss of coolant. Fig. 15 shows the temperature distributions of the optimized current lead for different times after stopping the helium mass flow completely. The behaviour of the warm end did not change very much, the maximum temperature reaches the 330 K level after 20 minutes. This will be completely different in case of a high conductivity copper current lead, e.g. the CERN-LHC lead, as will be shown in chapter 5.

The shape of the distribution at the cold end changes fast, as can be seen in Fig. 16. After roughly two seconds, the heat loss has been increased from 2 Watts to more than 4 Watts. After two minutes one gets 15 Watts, while the maximum temperature changes by less than one Kelvin. In Fig. 17 resp. 18 the time dependence of the heat losses at the cold resp. the warm end and the maximum temperature - which is correlated to the voltage drop - are plotted. It should be mentioned that the optimum Fourier number has been choosen for this study.
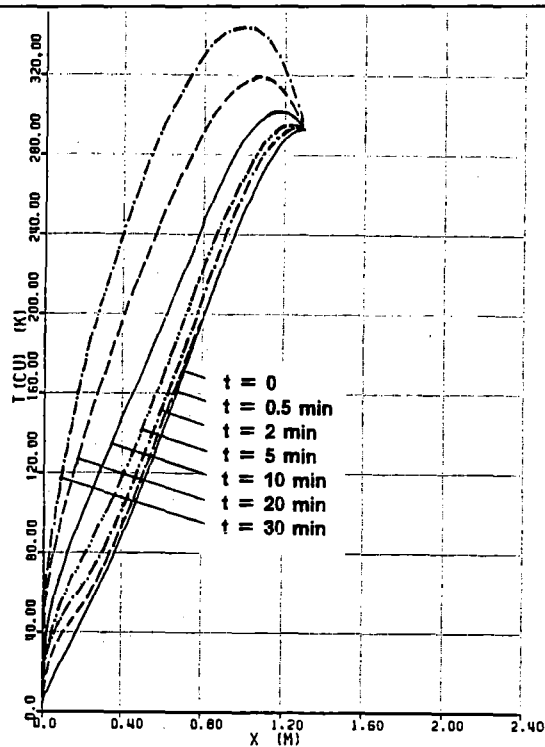
Figure 15.   Transient behaviour of an optimized current lead - temperature distribution
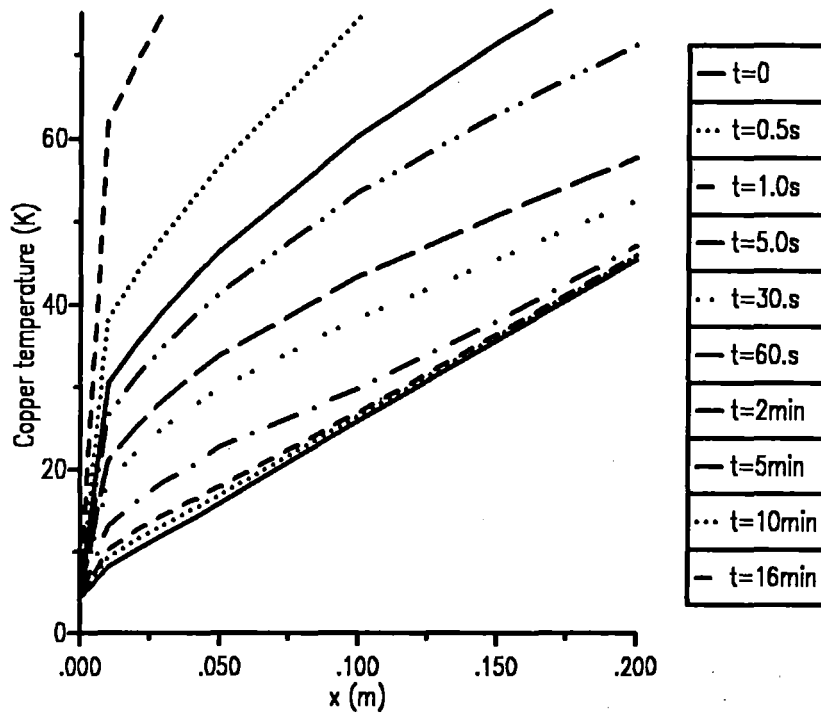
Figure 16. Transient behaviour of an optimized current lead - temperature distribution at the bottom end
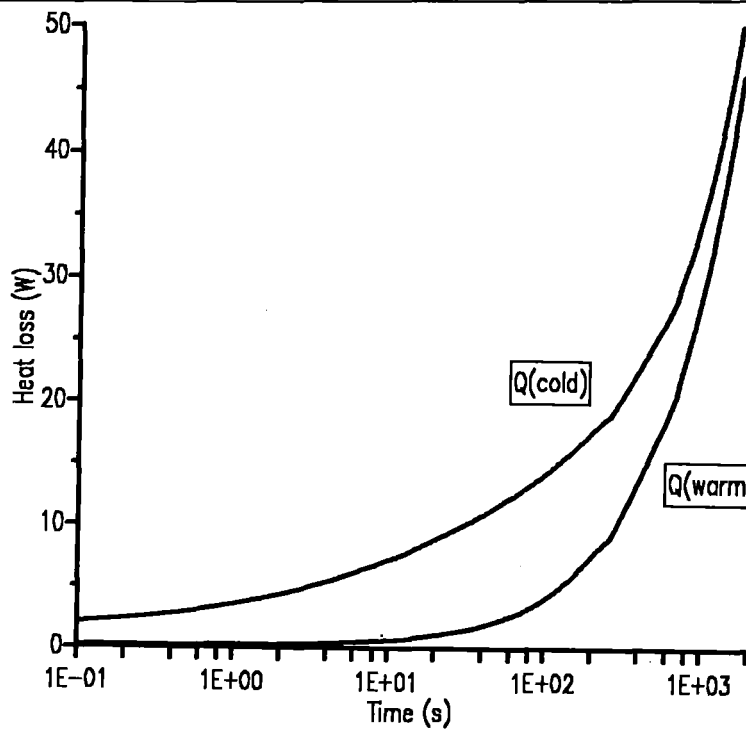
Figure 17. Transient behaviour of an optimized current lead: heat loss at the cold and at the warm end vs. time
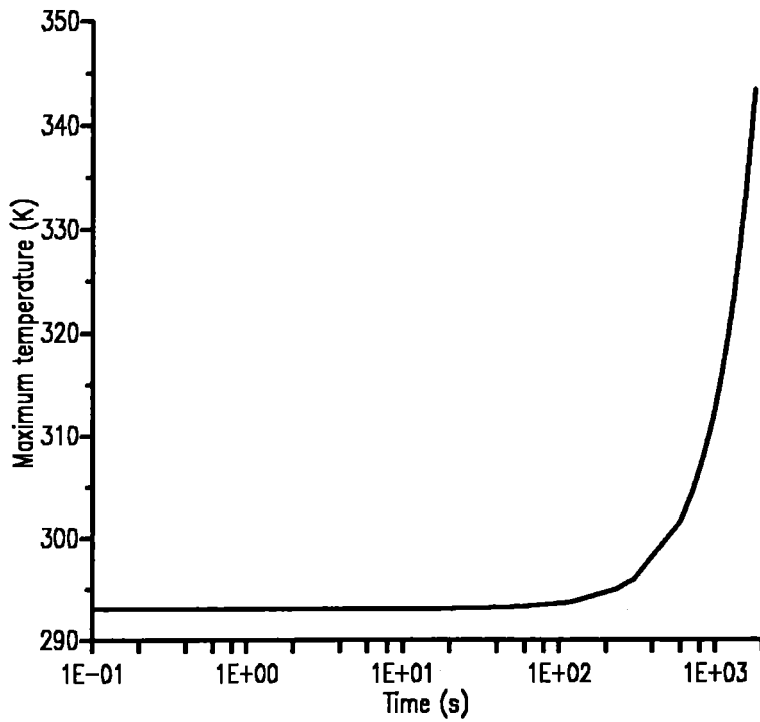
Figure 18. **Transient behaviour of an optimized current lead:** Maximum temperature vs. time

4.5 Accuracy and convergency studies

Now the effect of the tolerancy parameter TOL and the step length Δx will be presented. Fig. 19 shows the heat losses resp. the voltage drop along the current lead as a function of the step length Δx, while in Fig. 20 the same variables are plotted vs. the tolerancy parameter TOL (for definition see eq.(3.9)).
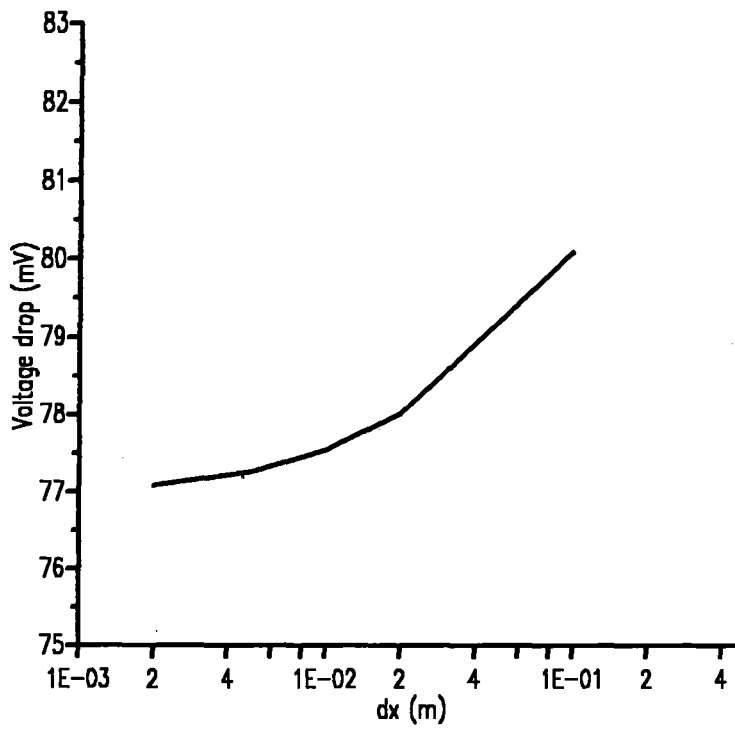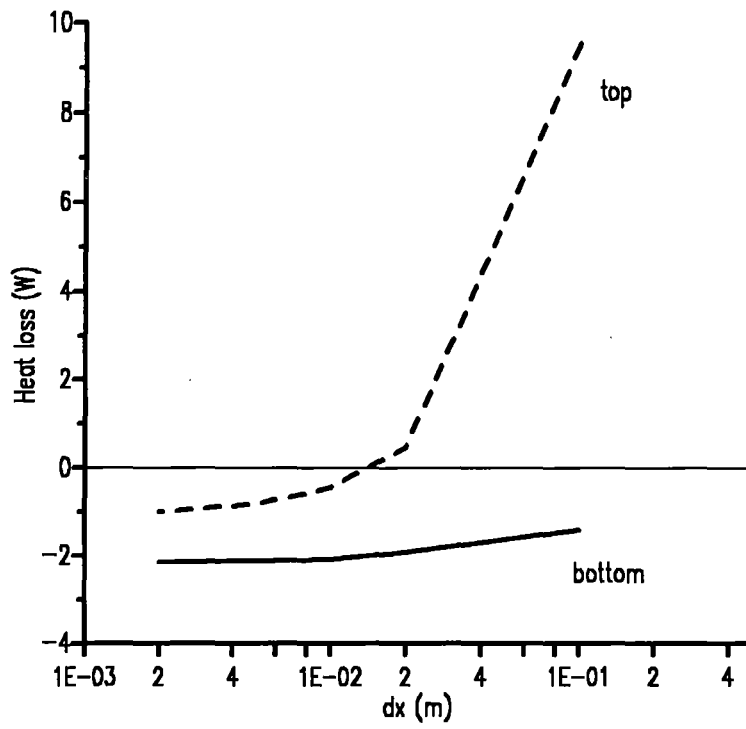
Figure 19. Accuracy and stability - Δx dependence:

top. heat loss at the cold and at the warm end vs. Δx

bottom. voltage drop vs. Δx
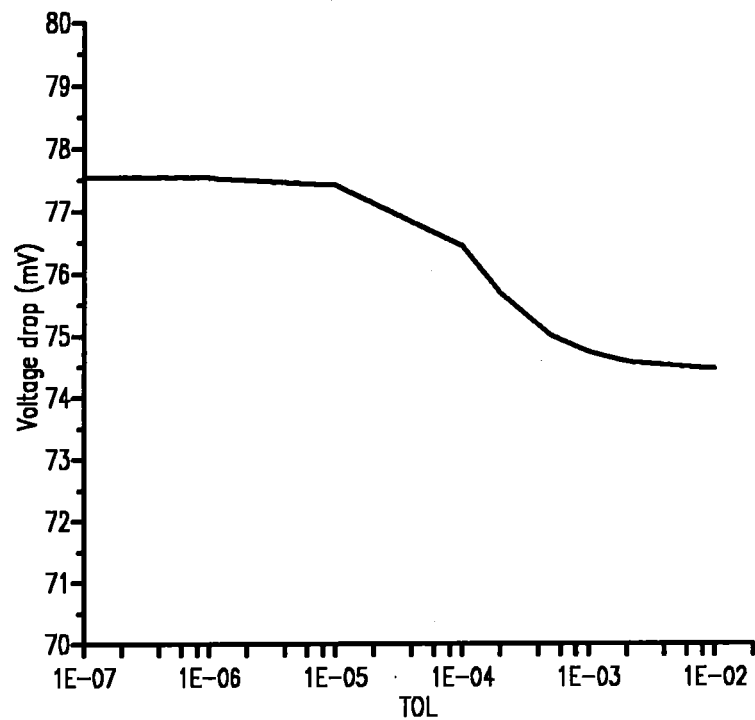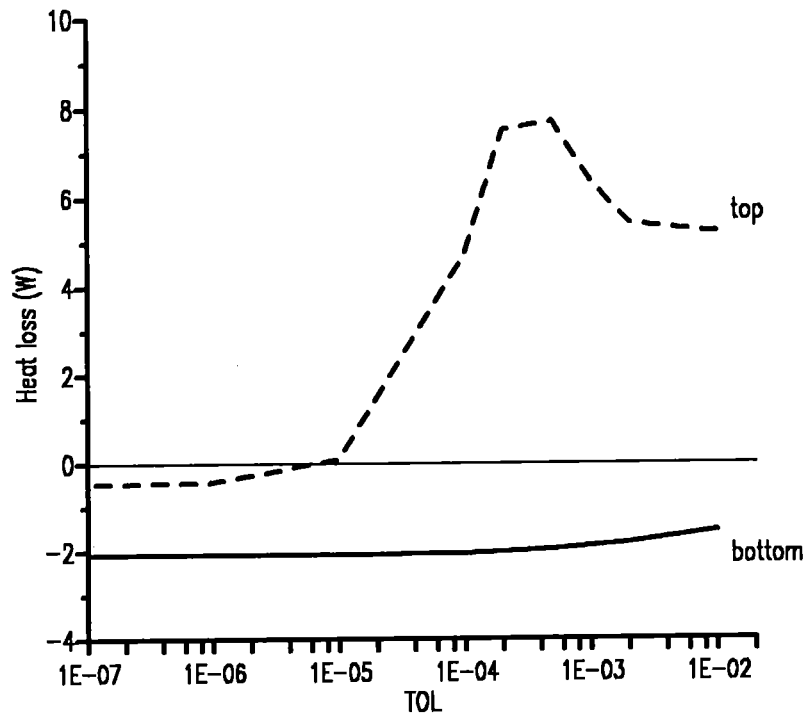
Figure 20. Accuracy and stability - TOL dependence:

top. heat loss at the cold and at the warm end vs. TOL

bottom. voltage drop vs. TOL

By looking in the distributions (Fig. 19 resp. Fig. 20) significant changes are obtained obove a step size of Δx = 0.01 m resp. a tolerancy of TOL = 10^{-5}.

In Fig. 21 the relative temperature difference between copper and helium is plotted as a function of the number of iterations, NIT, e.g.

$$RELTC = \sqrt{\sum_i \frac{1}{N} (T_{Cu,i} - T_{He,i})^2} .$$
(4.1)
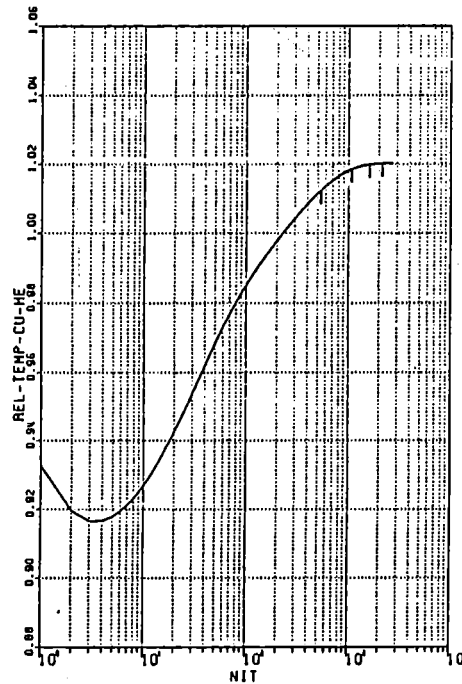
Figure 21. Accuracy and stability - relative temperature difference between copper and helium

As can be shown the variation of RELTC from the (i-1)-th to the i-th iteration corresponds to the variation of the temperature distribution, and of the heat losses, voltage drops etc. as well. NIT is a measure for the CPU-time needed to solve the problem and is directly correlated to the tolerancy, TOL. It is surprising how small values of TOL are needed to get almost no changes in the temperature distribution, or in RELTC as well. By looking in Fig. 22 the temperature distributions below a tolerancy of 10^{-5} coincide, whereas the distribution for TOL = 10^{-3} shows a slight difference.

40
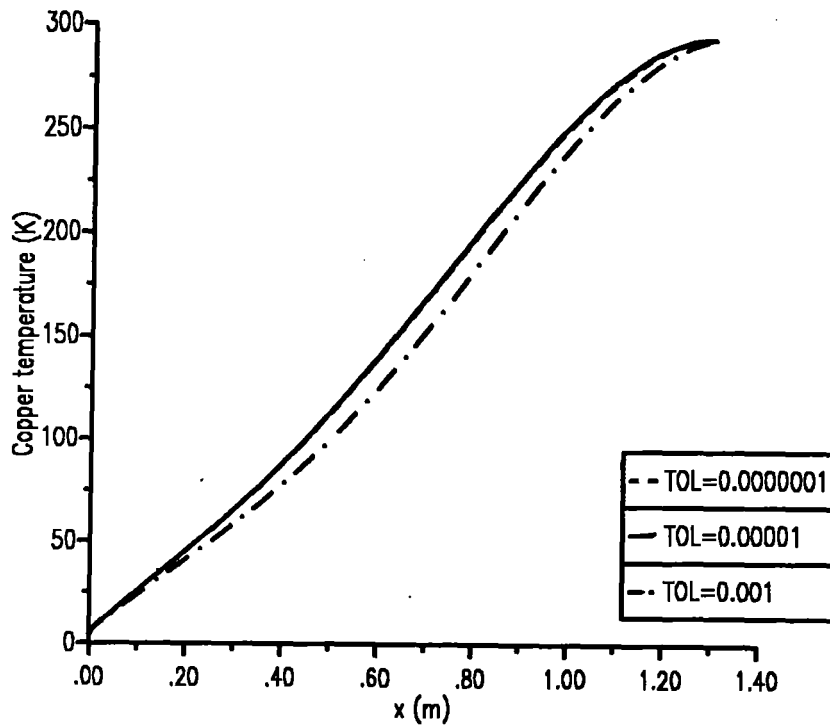
Figure 22. Accuracy and stability - temperature distributions for different TOL

As a result of this study the largest TOL resp. Δx has been used to get the results for all parameter change studies, which have been presented in this chapter to be sure that no significant change occurs at any parameter.

Chapter 5. Testing the code by calculating existing current leads

5.1 General remarks

One benchmark is the recalculation of already existing current leads which have different heat exchangers (hex):

- a 18 kA CERN-LHC current lead [18], and

- a 15 kA current lead for TORE SUPRA [19].

The differences are in case of the hydrodynamic model - the LHC-lead belongs to a "Dittus-Boelter"-type (parallel-flow), while the TORE SUPRA lead belongs to the cross-flow type -, and in case of the copper used - the LHC lead is made by high conductivity copper, while the TORE SUPRA one has been built by using low RRR copper -. This means that both models can be tested by a recalculation.

For both examples a comparison to results obtained with other codes has also been done. Two programs developed at CERN are used for this purpose. The first one (CLEAD10B) [18] has been written for one special problem and is therefore very difficult to handle for other purposes. For example the cold end losses are calculated by means of the mass flow and the enthalpy of the liquid helium. So the obtained result is always this input value. In addition the hydrodynamic properties are parametrized by assuming a constant Nusselt number for laminar flow (see eq. (2.10a)) resp. the Dittus-Boelter-equation for turbulent flow (see eq. (2.9)). The second code (GU2) [20] is more general with respect to material properties, but the helium data are also fixed. In addition the heat transfer coefficient at room temperature is needed, too.

Therefore both codes are used for recalculating the CERN-LHC current lead, while for the TORE SUPRA one only the latter code has been compared to CURLEAD. The results will be shown later on.

Before the different results are discussed, some attention is given to the question how to compare the calculation with the measurement data. The following two variables are defined for this purpose:

$$\chi^2 = \sum_{i=1}^{n}(T_{calc,i} - T_{data,i})^2,$$ (5.1)

and

$$\sigma = \frac{1}{n}\sqrt{\sum_{i=1}^{n}(\frac{T_{calc,i} - T_{data,i}}{T_{data,i}})^2},$$ (5.2)

where n denotes the number of measurement points, and the calculated temperatures are taken at the same location as the data. χ^2 "measures" the absolute deviation, i.e. it is independent of the temperature itself, while σ is more sensitive to small numbers, i.e. to deviations at the bottom end of the current lead. In the following when calculated and measured temperatures are compared, both numbers are given.

5.2 A 18-kA current lead for LHC

First some emphasis was given on the high conductivity current lead, developed at CERN for testing superconducting magnets for the proposed Large Hadron Collider LHC [25].The heat exchanger part consists of a stack of 78 copper finned foils, each 30 mm wide and 0.53 mm thick, and chemically etched at 0.23 mm to form a staggered arrangement of buttons. More details are presented in [18]. In Tab. 4 the parameters relevant for the recalculation are given. It should be mentioned that these numbers belong only to the pure heat exchanger, but not to the whole current lead, including the cold and the warm end terminals. For the latter one, a separate calculation has been done and will be presented after the results of the heat exchanger itself.

Parameters	Unit	Value
I	A	18000
L_{hex}	m	1.0
L_{tot}	m	1.5
A_{Cu}	m^2	$7.48\ 10^{-4}$
P_{co}	m	3.51
A_{co}	m^2	$4.52\ 10^{-4}$
$\dot{m}$	$\dfrac{g}{s}$	0.952
f		0.5
RRR		78
$\dfrac{L\,I}{A_{Cu}}$	$\dfrac{A}{m}$	$2.4\ 10^7$

Table 4.   Design parameters for the high conductivity copper CERN-LHC current lead

Fig. 23 shows the temperature distribution obtained by using the parameters written in Tab. 4. The agreement between the calculated and the measured temperatures are reasonable, except the region around 60 K. By changing the residual resistivity ratio to 97, one gets a better agreement. Tab. 5 summarizes the results obtained with different codes and also different algorithms. It should be noted that in case of the Runge-Kutta-algorithm the heat transfer efficiency f was adjusted just to get an upper temperature of 266 K. It was decided to use an RRR of 97 instead of 78. In Fig. 24 the temperature distributions obtained with the different computer codes and/or different algorithms are shown. The measurement data are also plotted for comparison. The conclusion is that all codes give similar results.
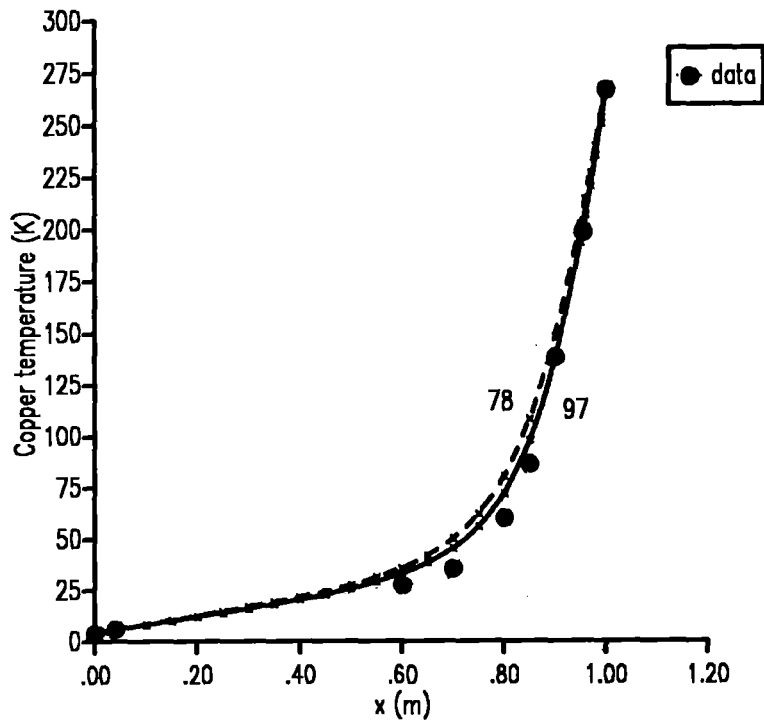
Figure 23. Temperature distribution of the heat exchanger - RRR = 78 resp. 97: CERN LHC current lead
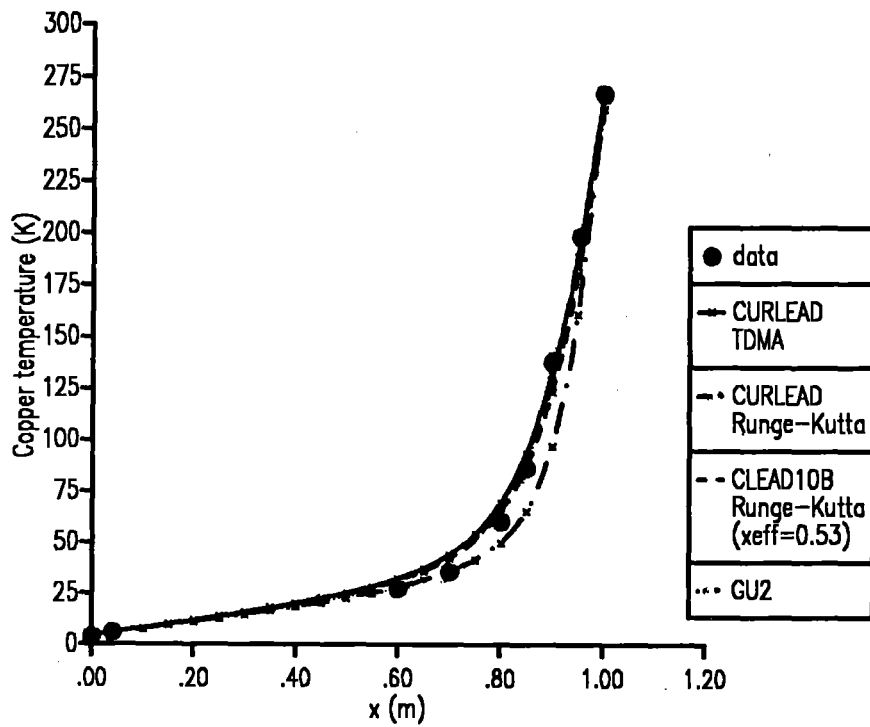
Figure 24. Temperature distributions obtained with different algorithms and/or codes: CERN LHC current lead

RRR	f	Q_{bot}	ΔU	χ^2	σ	Remarks
		[W]	[mV]		[%]	
78	0.55	-18.71	47.67	2472	8.9	CURLEAD with TDMA
97	0.55	-21.46	42.46	900	5.9	CURLEAD with TDMA
78	0.37	-19.90	43.31	805	6.1	CURLEAD with Runge-Kutta
97	0.57	-19.90	37.66	230	3.4	CURLEAD with Runge-Kutta
78	0.29	-19.90	32.0			CLEAD10B with Runge-Kutta
97	0.50	-19.90	28.66			CLEAD10B with Runge-Kutta

Table 5.   Summary of results of calculations for the LHC heat exchanger and comparison with the measured data

In Fig. 25 the temperature distribution of the heat exchanger is shown and compared with the measurements. But in addition a combined calculation was done including the warm end terminal, which leads to a longer length of L = 1.26 m. The parameters needed for modelling the warm end are the length and the copper cross section, but no cooling was assumed [21] . The effect of the poor cooled end can be clearly seen, and it is remarkable that the calculation can reproduce this behaviour. It should be noted that it is not possible to model the warm end together with the heat exchanger by using the CERN program - the Runge-Kutta method leads to unrealistic results e.g. extremely high temperatures. The reason is already given in chapter 3.

In Tab. 6 the results for the heat losses, the voltage, and the pressure drops obtained by the computer code are compared to the measured ones. The pressure drops have been calculated only for the heat exchanger, therefore the numbers obtained with CURLEAD for the whole current lead are the same and they coin-
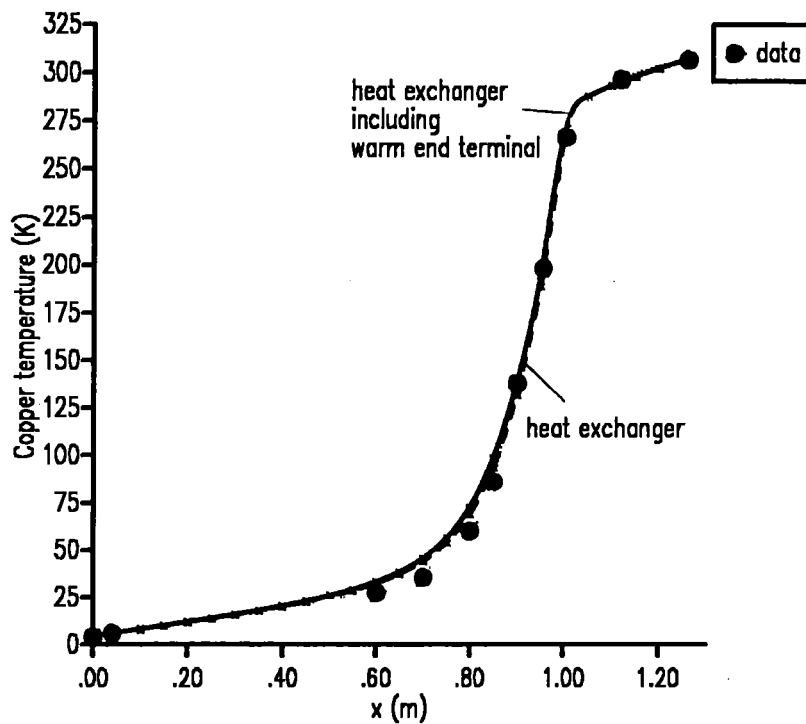
Figure 25. **Temperature distributions of the heat exchanger resp. the current lead:** CERN LHC current lead

cide with the calculations with CLEAD10B. For the discrepancies between the measurements and calculations for the voltage and pressure drops it has to be concluded that more informations on the warm end design are necessary.

Remarks	Calculations			Measurements		
	Q_{bot}	ΔU	Δp	Q_{bot}	ΔU	Δp
	$[W]$	$[mV]$	$[mbar]$	$[W]$	$[mV]$	$[mbar]$
heat exchanger (CURLEAD)	-21.24	42.46	22.2			
heat exchanger (CLEAD10B)	-19.9	28.66	22.4			
current lead (CURLEAD)	-21.69	51.95	22.2	-19.9	62.0	45.

Table 6. **Comparison of calculated and measured data:** CERN-LHC current lead

In Fig. 26 the heat transfer coefficient h(T) resp. the Reynolds number Re are plotted for the heat exchanger part of the current lead as a function of temperature. The heat transfer coefficient is surprisingly large, but also the hydraulic diameter d_H is very small.
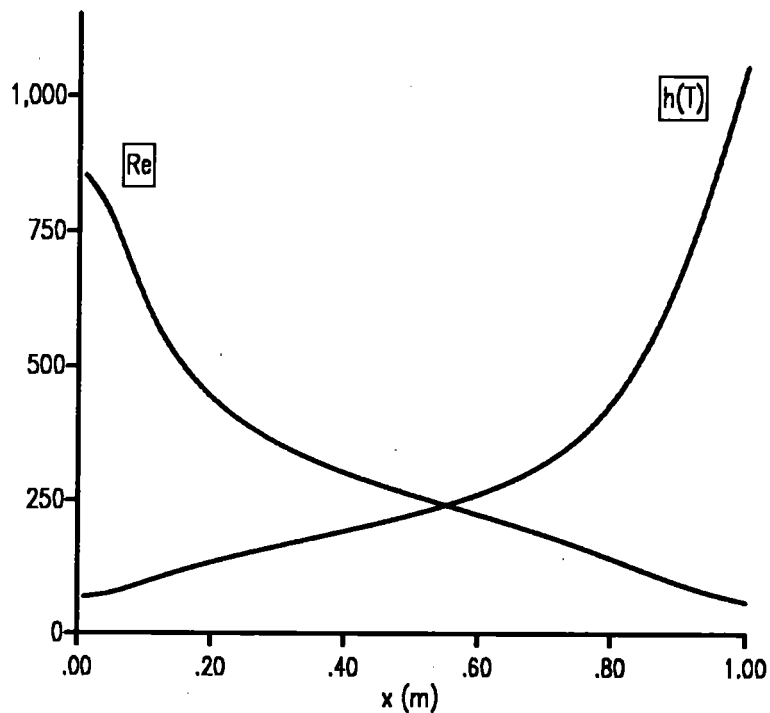
Figure 26. **Reynolds number resp. heat transfer coefficient** $(W/(m^2 K))$: CERN LHC current lead

Now the transient behaviour of the CERN current lead will be discussed. Fig. 27 shows the maximum temperature of the current lead as a function of time. If the time scale is compared to that of Fig. 15, an extremely sharp increase of T_{max} is observed which leads to a time scale of 2 minutes for reaching the melting point of solder.
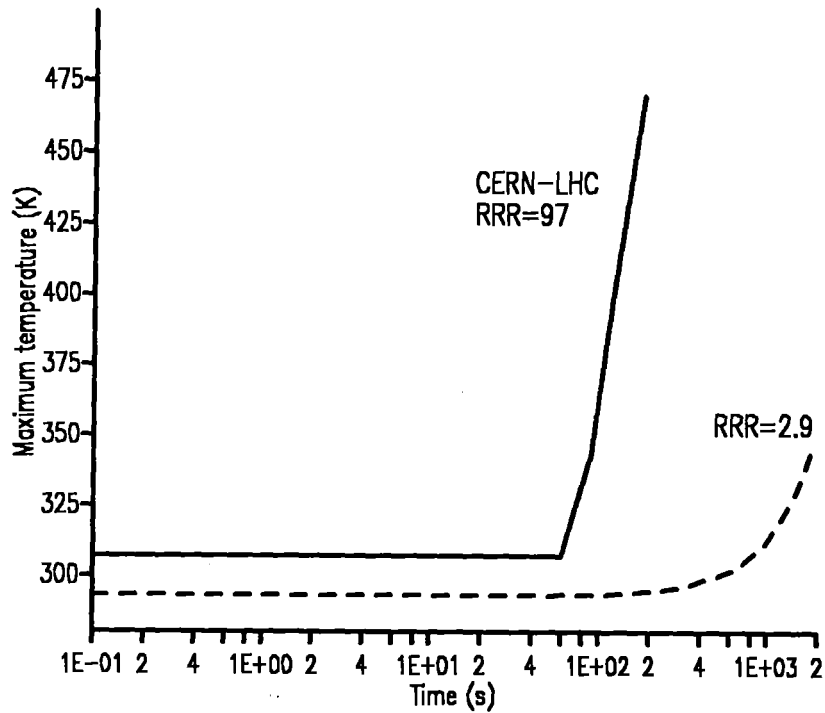
Figure 27. **Maximum temperature vs. time:** CERN LHC current lead

Fig. 28 shows the temperature distributions for different times after switching off the helium cooling completely. First a similar behaviour is seen at the cold end than for the current lead described in chapter 4 in very detail. But in addition a peak in the region of the connection between the heat exchanger and the warm end terminal has been obtained, while the warm end itself doesn't change its shape very much.

As a conclusion one can state that a high conductivity current lead allows a higher current density but gets less stable in case of cooling or current failures.
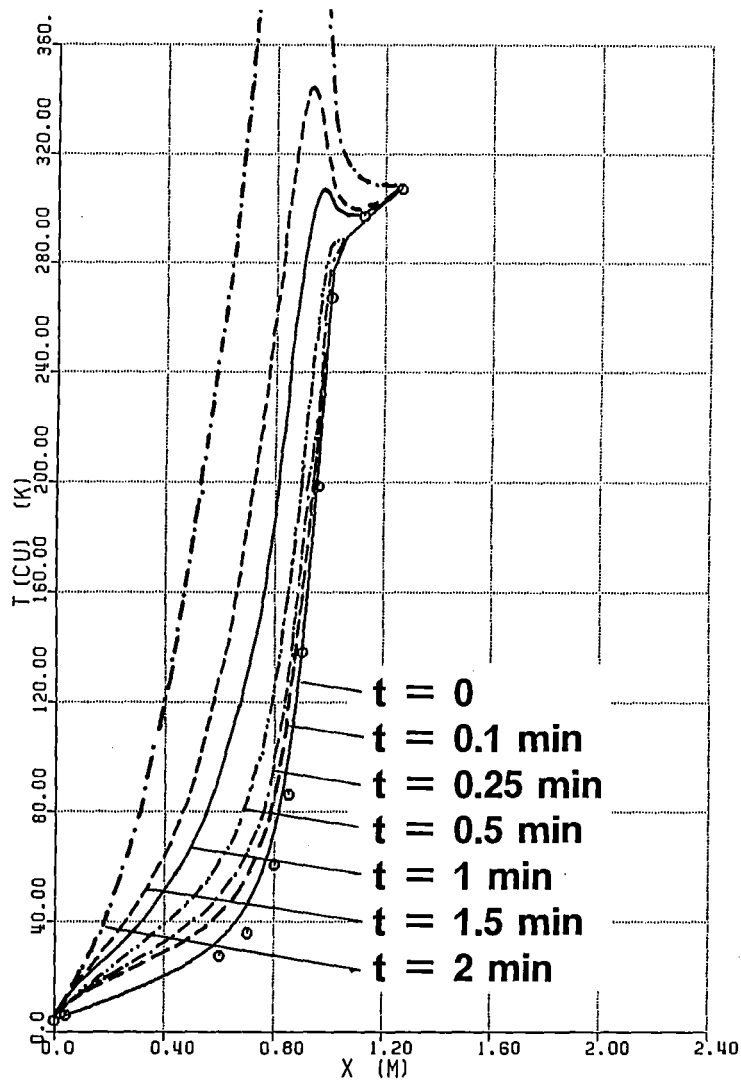
Figure 28. Temperature distributions of the LHC current lead - transient case: CERN LHC current lead

5.3 A 15-kA current lead for TORE SUPRA

The second example of a recalculation is a 15 kA current lead made of low conductivity copper and built for the fusion experiment TORE SUPRA at CEA, Cadarache. The heat exchanger part consists of a copper bar and a large number of round plates made of copper wire grating - like used in a fly screen - which are arranged and soldered around the bar (see also Fig. 3). Details are given in [19]. In Tab. 7 the parameters necessary for the calculation are summarized.

Parameters	Unit	Value
I	A	15000
$L_{h.e.}$	m	1.20
L_{tot}	m	1.58
A_{Cu}	m^2	$18.1\ 10^{-4}$
P_{co}	m	5.06
A_{co}	m^2	$7.90\ 10^{-4}$
d_a	mm	0.14
s_1	mm	0.35
s_2	mm	1.13
$\dot{m}$	$\dfrac{g}{s}$	1.0
f		0.5
RRR		~ 5
$\dfrac{LI}{A_{Cu}}$	$\dfrac{A}{m}$	$1.08\ 10^7$

Table 7.   Design parameters for the low conductivity copper TORE SUPRA current lead

For the calculation of the heat transfer coefficient the cross-flow model described in detail in chapter 2 is valid. A comparison of these calculations to the results obtained by the parallel-flow model will be given

The sensitive variable is the friction factor ζ (see eq. (2.12) resp. eq. (2.21)), which is related to the Reynolds number Re and leads to the pressure drop $\frac{dp}{dx}$. In Fig. 29 ζ is plotted vs. Re for both models. Due to the large difference it should be possible to distinguish experimentally by measuring the pressure drop along the heat exchanger and calculating the hydraulic diameter either by means of the equations representing the geometry in case of the model, or by means of the helium cooling channel area and the cooling perimeter. Afterwards the Reynolds number and the friction factor can be calculated, the latter one by means of the measured pressure drop.

By using the parallel-flow model a much lower pressure drop has been calculated whereas the corresponding number obtained by the cross-flow model is too high (see last entry in Tab. 9). Because both numbers are sensitive to the exact geometry one can adjust them by changing for example the radial wire distance slightly.
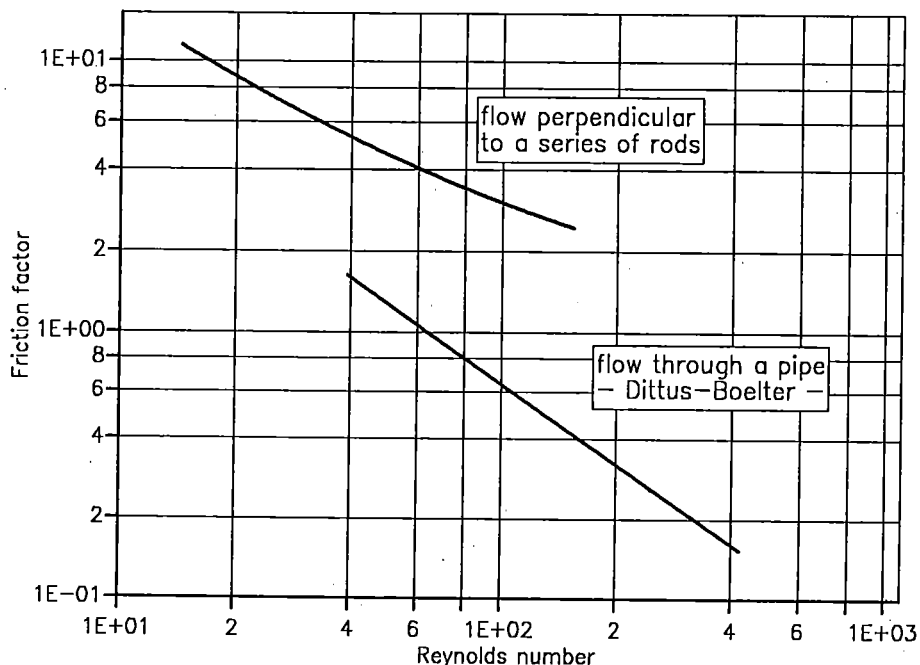
Figure 29. **Friction factor vs. Reynolds number for the different models:** TORE SUPRA current lead

The difficulty for the recalculation comes from the fact that the residual resistivity ratio RRR is not well known, and there exist also no experimental data for the thermal conductivity. On the other hand measurement data are available for at least three currents,

- 0 kA - case A.
- 10 kA - case B, and
- 15 kA - case C,

Due to the inaccuracy of knowing the RRR, several computer runs have been done varying the RRR and the thermal conductivity as well. Fig. 30 shows the thermal conductivities for an RRR range of 5 to 7.5. Although there is no big difference the temperature distributions obtained by using these distributions are significantly different. In Fig. 31 the temperature distributions for RRR = 5, 6.5, and 7.5 are plotted for case C. In addition the measurement data are also shown for comparison.
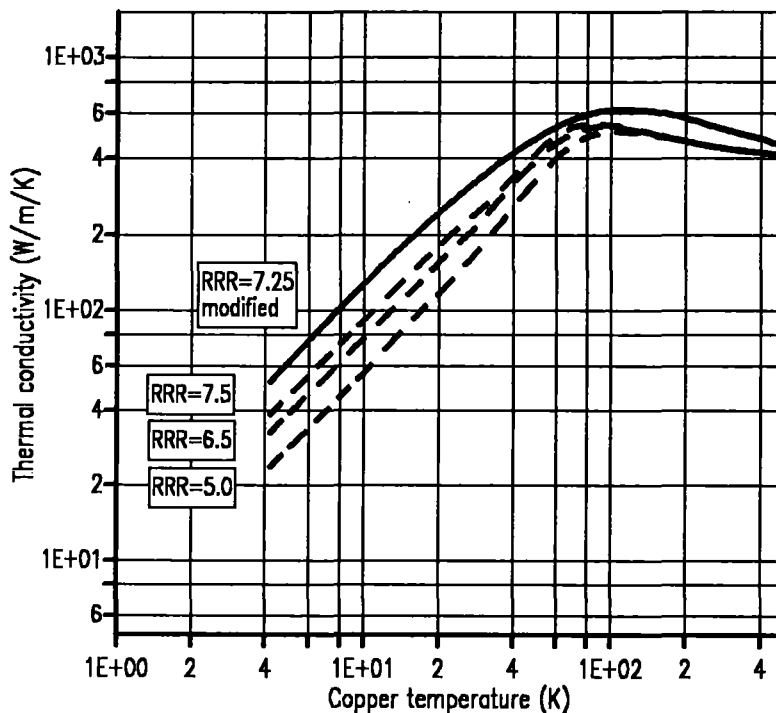
Figure 30.   Thermal conductivities for RRR = 5.0, 6.5, and 7.5:   TORE SUPRA current lead
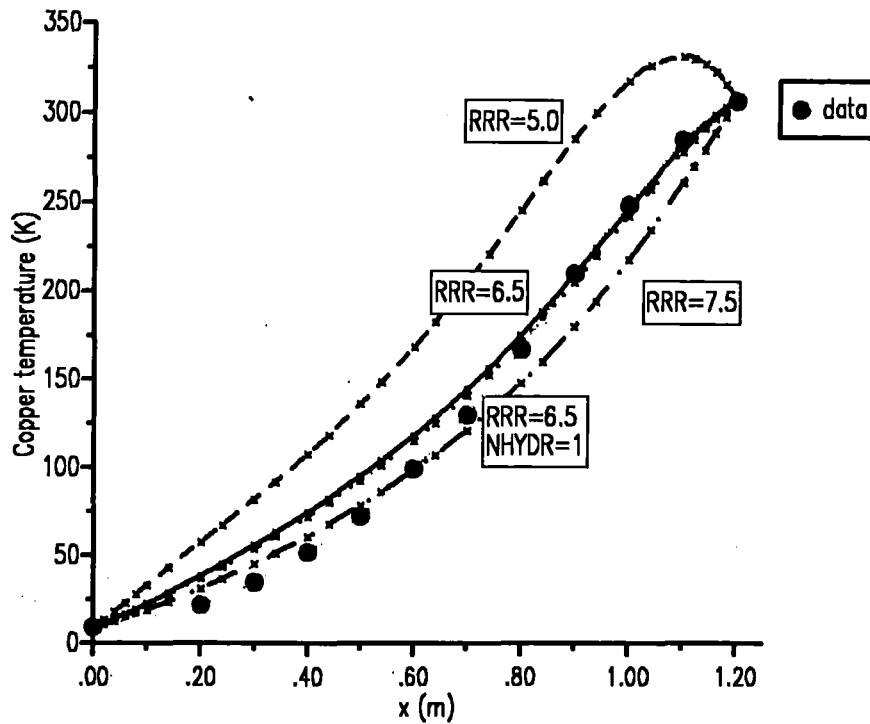
Figure 31. Temperature distibutions for RRR = 5, 6.5, and 7.5: TORE SUPRA current lead

The bottom and top ends are made of high conductivity copper and connected to the low conductivity heat exchanger by screw threads. Since CURLEAD offers the possibility to calculate the current lead including its cold and warm end terminals, but only with one common thermal conductivity and electrical resistivity, the following assumptions are made to get the results for the whole current lead:

• for the warm end terminal the dimensions are used as given in the design drawings, because the material properties at room temperature are more or less the same for low and high conductivity copper.

• for the cold end terminal, which is partly covered by superconducting wires, the effect of the high conductivity copper was taken into account by using a shorter length.

In the following all distributions and numbers are obtained for the whole current lead.

Tab. 8 contains the measured values for the three cases, while Tab. 9 summarizes the calculation results, including the consistency parameters χ^2 and σ, as defined in eq. (5.1) and (5.2). The only parameter change is the RRR, and the thermal conductivity, respectively.

I	$\dot{m}$	Q_{bot}	ΔU	Δp
[kA]	$[\frac{g}{s}]$	[W]	[mV]	[mbar]
0	0.44	9.2	0.0	13.5
10	0.68	14.2	47.15	24.9
15	0.99	20.7	89.3	54.4

Table 8.   Measurement data of the TORE SUPRA current lead

I	$\dot{m}$	RRR	Q_{bot}	ΔU	Δp	χ^2	σ
[kA]	$[\frac{g}{s}]$		[W]	[mV]	[mbar]		[%]
thermal conductivity parametrization by Lock							
0	0.44	5.0	0.0	0.0	15.8	9129	11.1
0	0.44	6.0	0.0	0.0	16.2	4586	8.1
0	0.44	6.5	0.0	0.0	16.4	4269	6.8
0	0.44	7.0	0.0	0.0	16.7	3720	5.3
0	0.44	7.5	0.0	0.0	16.4	7024	6.9
10	0.68	6.5	5.6	56.4	42.4	1970	6.7
15	0.99	6.5	8.6	103.0	99.1	2176	6.4
thermal conductivity parametrization modified							
0	0.44	7.25	2.6	0.0	20.5	703	3.7
10	0.68	7.25	13.8	55.7	45.7	2239	8.7
15	0.99	7.25	17.9	101.2	102.0	2621	7.7
15*	0.99	7.25	27.5	100.0	37.8	2462	7.5

Table 9.   Calculation results of the TORE SUPRA current lead: * = Dittus-Boelter

Due to the poor agreement between the calculated and measured temperature distributions of case A (0 kA), the thermal conductivity was modified, as has been also shown in Fig. 29.

Using this conductivity distribution all three cases have been calculated, and plotted together with the measured values, e.g. Fig. 32 for case A, and Fig. 33 resp. 34 for the 10 kA and 15 kA case.
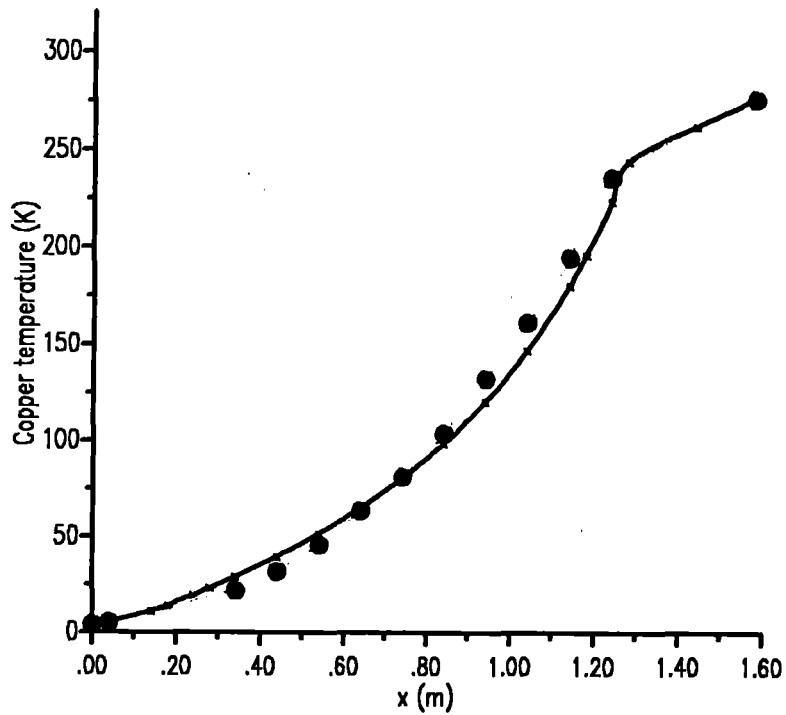
Figure 32.   Temperature distibutions for I = 0 kA: TORE SUPRA current lead
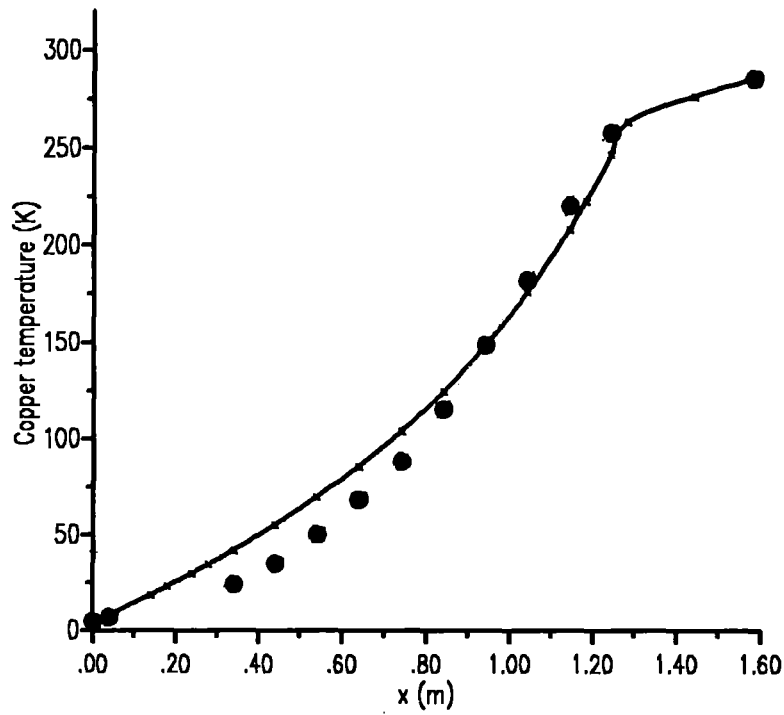
Figure 33. **Temperature distibutions for I = 10 kA:** TORE SUPRA current lead
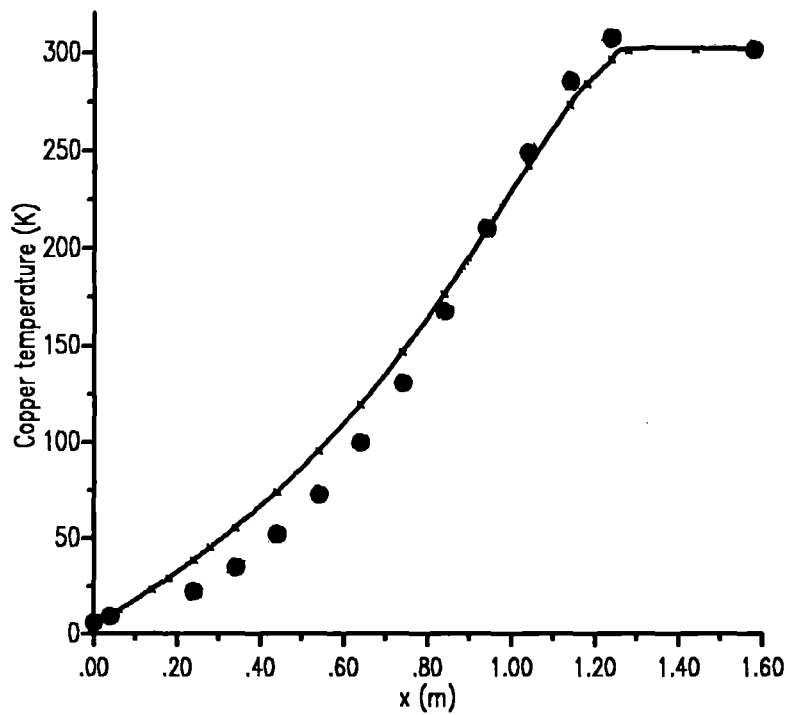
Figure 34. **Temperature distibutions for I = 15 kA:** TORE SUPRA current lead

The results obtained with CURLEAD are also compared to those of another code GU2 [20]. The latter one needs the heat transfer coefficient at room temperature as input. Therefore this has been calculated by CURLEAD and then put into GU2. Fig. 35 shows the temperature distributions which corresponds to both codes.
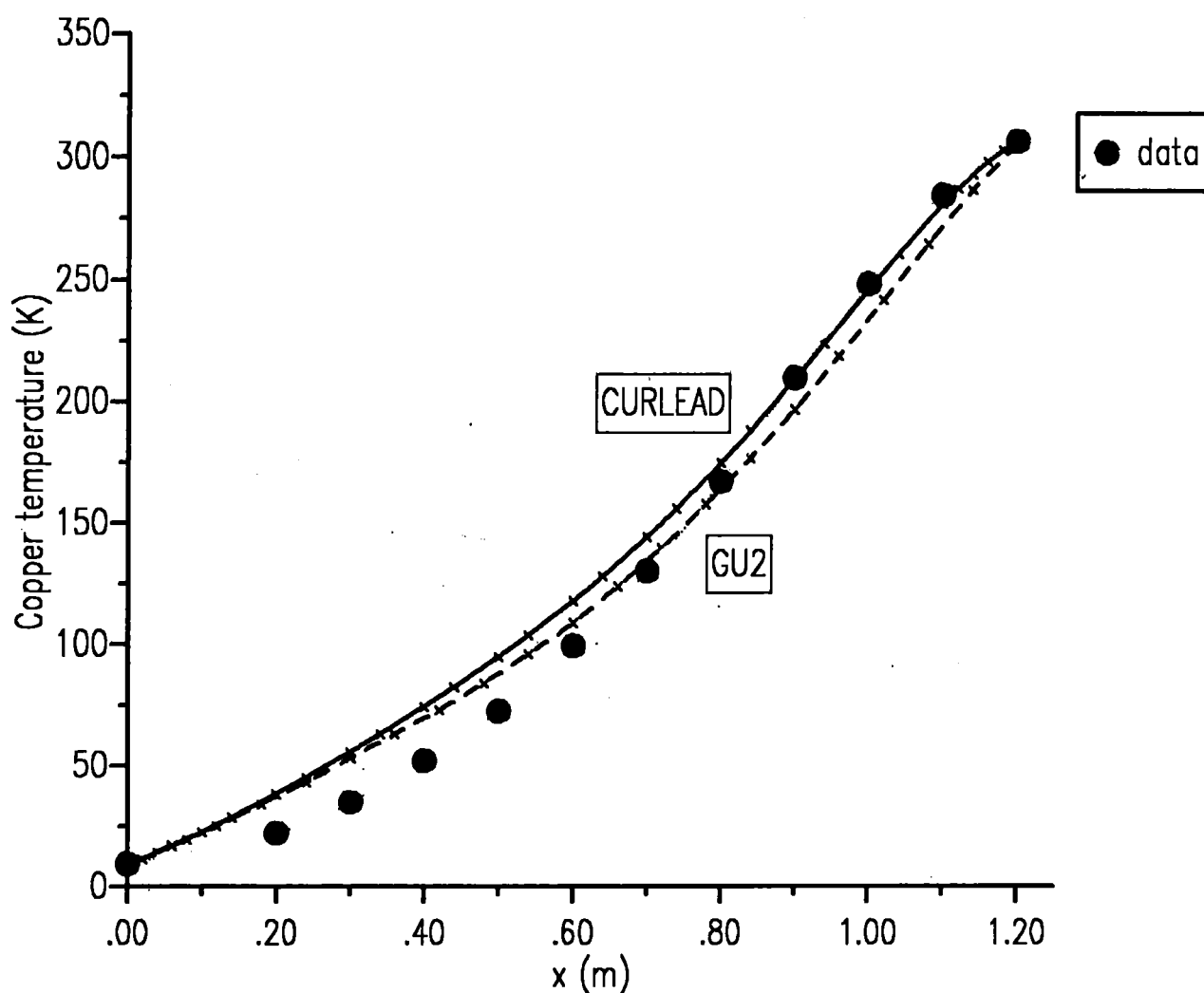
Figure 35. **Temperature distibutions for** I = **15 kA - comparison of different codes:** TORE SUPRA current lead

The measured and calculated distributions are in modest agreement. Especially in the lower temperature range the results of CURLEAD are significantly higher.

But this can easily be explained by the uncertainty of the thermal conductivity and electrical resistivity.

Chapter 6. Optimization of the POLO current lead

6.1 General remarks

In this paragraph the optimization procedure for a 30 kA current lead for the superconducting poloidal field coil POLO will be presented [4]. Preparatory work has been done by [22]and [23]. Special attention will be given to the forced flow cooling mode of the lead, and to the problem of optimizing the length of the current lead for different running conditions e.g.

- zero current,
- 17 kA,
- 23 kA, and
- 30 kA.

As has already been shown (eq. (2.2)), the optimized length of the lead depends on the operating current for a given cross section and a given copper material. With other words, it is principally impossible to optimize the length of the heat exchanger, including minimizing the helium mass flow, for all cases. For example the length of the lead should theoretically extremely long for zero current, while for a high excess current, e.g. 30 kA, the length has to be reduced drastically (from 15 kA to 30 kA by a factor of two). Of course it is possible to balance the "wrong" length with a higher mass flow (needed at the bottom end), which will be expensive, and also lead to a high heat loss at the warm end terminal. The latter one would lead to a too low copper temperature at the warm end and therefore to an "ice"-effect, which could reduce the breakdown-voltage in a pulsed current mode.

In most applications the optimization has been done for a definite running condition. In case of

- accelerator magnets (e.g. Tevatron [24], HERA [26], LHC [25], SSC [27], [28]): running time is much larger than the filling and accelerating times,
- toroidal field coils for fusion reactors (NET [1]): burning time is much larger than the running up and down times,
- toroidal field coils for experiments (LCT [29]): variable running conditions,

60

• labaratory magnets: variable running conditions.

In case of a poloidal field coil which is expected to run in a pulsed current mode, the key point in the design is the consideration of the losses at the cold **and** at the warm end terminals, because both ends define the parameters of the current lead.

In addition it was decided to built a current lead without a helium bath (=reservoir), but to cool it with forced flow helium at a pressure of four bars, because the helium capacity is much higher at four bars than at one bar. This forced-flow cooling mode under high pressure (4 - 10 bars) has the advantage that it will be relevant for the Next European Torus, NET [1]

Nevertheless the optimization procedure was done in the way described in the next chapter.

6.2 Optimizing of the length with respect to the helium mass flow

Consider first the real heat exchanger which consists of a copper bar with a cross section of 38.5 cm^2, and a cooling perimeter of 11.5 m, which will be realised by a large number of round copper plates, 135.7 mm outer diameter, with several thousand holes of 1.6 mm in diameter, and a plate distance of 2 mm. The nominal current was assumed to be 23 kA. The residual resistivity ratio RRR was set to 6.5.

Due to the geometry of the heat exchanger it was decided to use the hydrodynamic model which describes the flow perpendicular to a series of rods instead of the Dittus-Boelter equation. Therefore an equivalent rod diameter, and its correspondent transversal rod distance as well, is needed, which leads to a transformation of the plate with holes to a plate made by a number of rods crossing each other.

Tab. 10 summarizes the geometrical parameters which are used for the calculations presented here. Fig. 36 shows a top view of the copper plate which serves as a heat exchanger. More details including the production procedure and the design drawings are given in [30].

Parameters	Unit	Value
I	A	23000
A_{Cu}	m^2	$38.5 \ 10^{-4}$
P_{co}	m	11.5
A_{co}	m^2	$35.0 \ 10^{-4}$
d_a	mm	1.231
s_1	mm	2.5
s_2	mm	2.0
f		0.5
RRR		6.5

Table 10. Design parameters for the POLO current lead
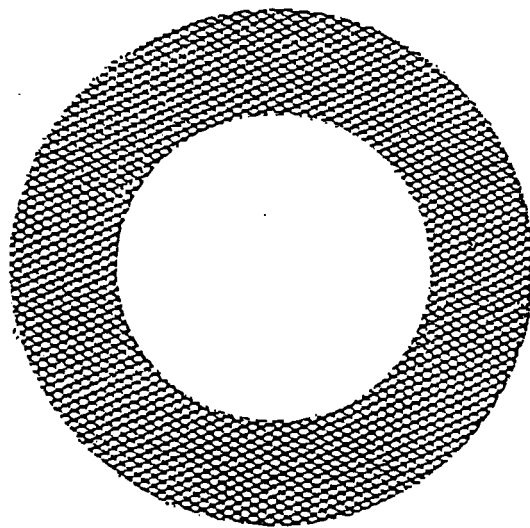
Figure 36. Top view of the copper plate for the heat exchanger: POLO current lead

Fig. 37 shows a schematic view of the total current lead, consisting of the heat exchanger, $I_B + I_C$, the cold and warm end terminals, I_B resp. $I_E + I_F$, and the superconducting bus, I_A. A scheme of the helium mass flow is also shown.
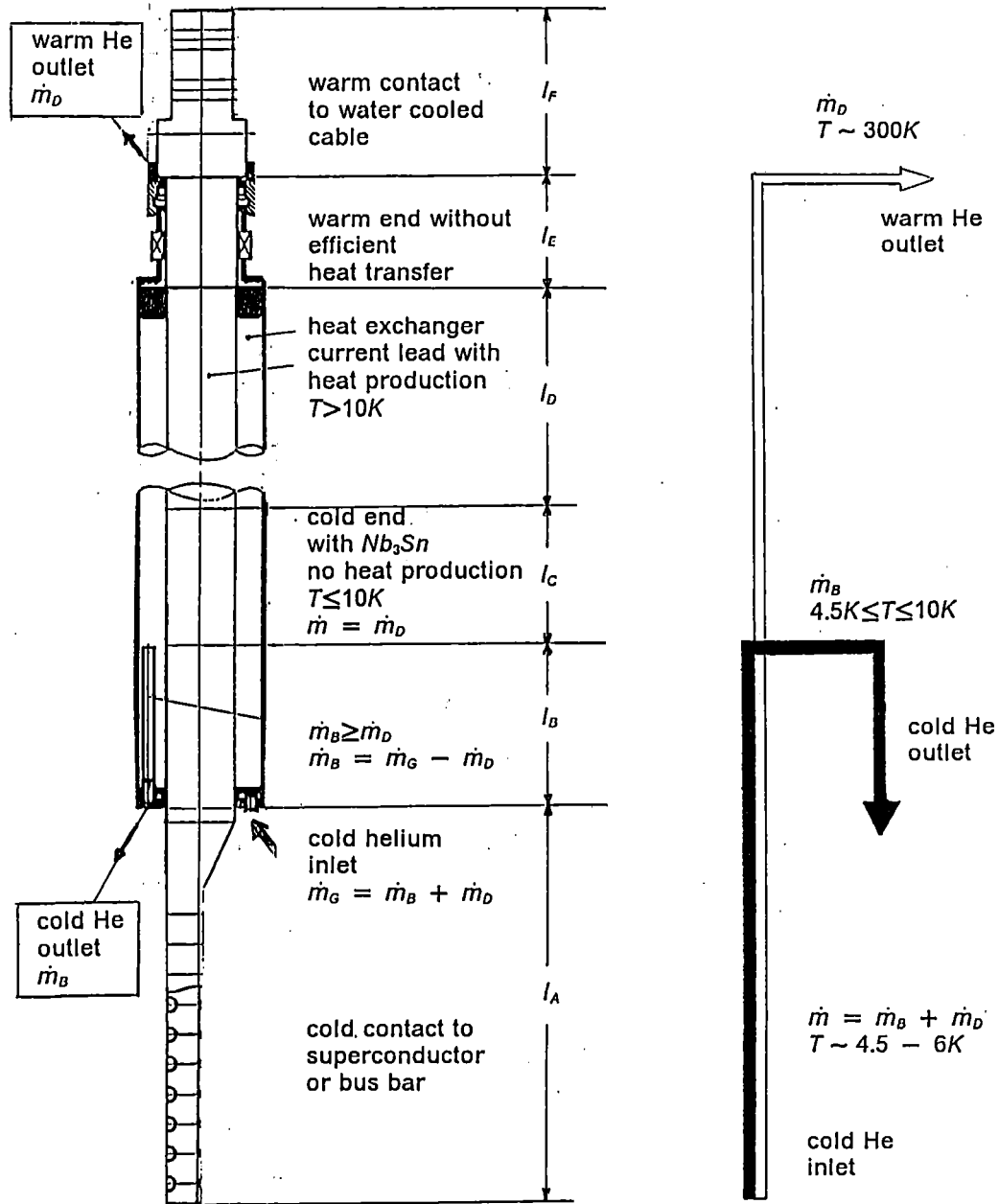
Figure 37. **Schematic view of the POLO current lead (left) resp. mass flow scheme (right)**

First the length of the heat exchanger was fixed to 1.9 m, and the helium mass flow was varied. In Fig. 38 the heat loss at the bottom (cold-) end is plotted as a func-

tion of the mass flow. In addition the heat loss obtained for the so called "self cooling condition" is also shown. Self-cooling condition means that the helium gaz which is produced by the heat loss is used to transfer the heat load over the whole length to the warm end, e.g.

$$Q_{cold} = \dot{m} \, \Delta H, \qquad (6.1)$$

where

ΔH = latent heat of helium at 4.2 K $(\frac{J}{kg})$.

The result of this study was the mass flow needed for the self-cooling condition. No attention was given to the top (warm-) end terminals so far.
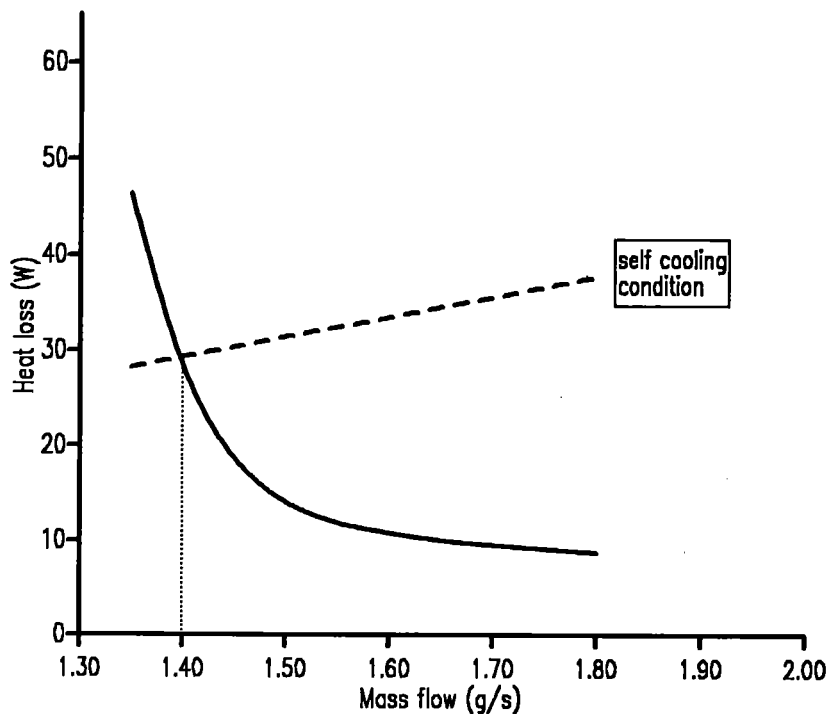
Figure 38. Heat loss at the bottom end vs. helium mass flow: POLO current lead

The next step was the variation of the heat exchanger length with respect of the heat loss at both ends. While the loss at the bottom end was only slightly changed during this study the heat loss at the upper terminal was very sensitive (as already described in chapter 4). At the end of the second step of the parameter study the optimum length and the mass flow, leading to the self cooling condition, were obtained.

Third, the cold end terminal was added, which means that a small part of the original heat exchanger was used, but the heat production was "switched off" which means that a number of superconducting wires are put in parallel, i.e. the copper bar only serves as a conductor for the heat loss at the end of the heat exchanger itself. The copper plates are used to increase the perimeter for the heat transfer to the helium. Together with the increase of the helium pressure from one bar to four bars the calculation was done und resulted in a net heat loss of roughly zero, e.g. all the produced and conducted heat was transferred to the coolant. A second calculation was done where the internal heat generation was "switched on", e.g. no superconducting wires are used. Fig. 39 shows the temperature distribution obtained after this step of the study for the bottom end region, without (full line) and with (dashed line) internal heat generation.
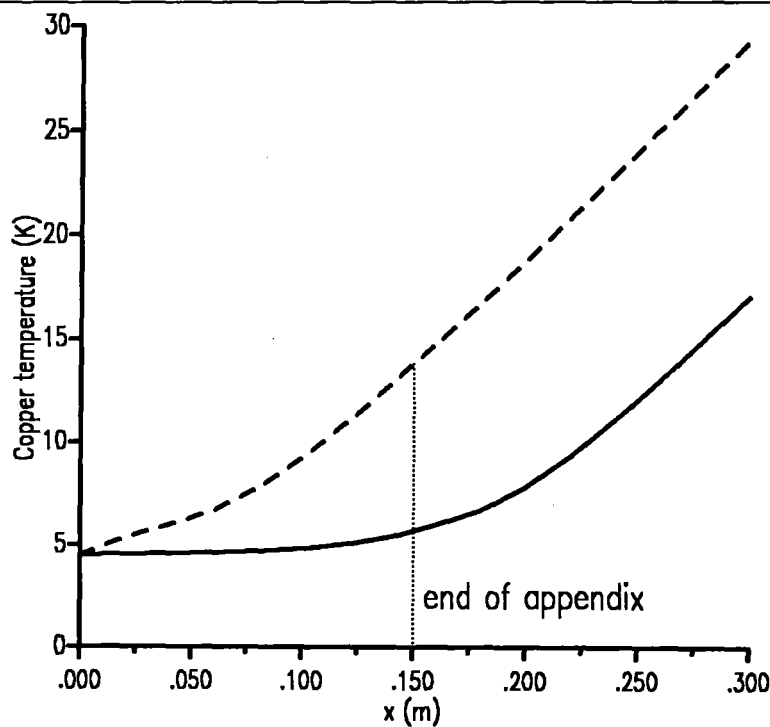
Figure 39. **Temperature distribution of the bottom end region of the heat exchanger:** Heat generation off (full line) resp. on (dashed line)

At the last step the warm end terminal was added, which led to an increase of the maximum temperature at the end of the heat exchanger. In Fig. 40 the temperature distributions are plotted with (full line) and without (dashed line) the warm end terminal. Consequently its length was further reduced until roughly zero slope has been got at the upper end.

The resulting parameters are summarized in Tab.11.
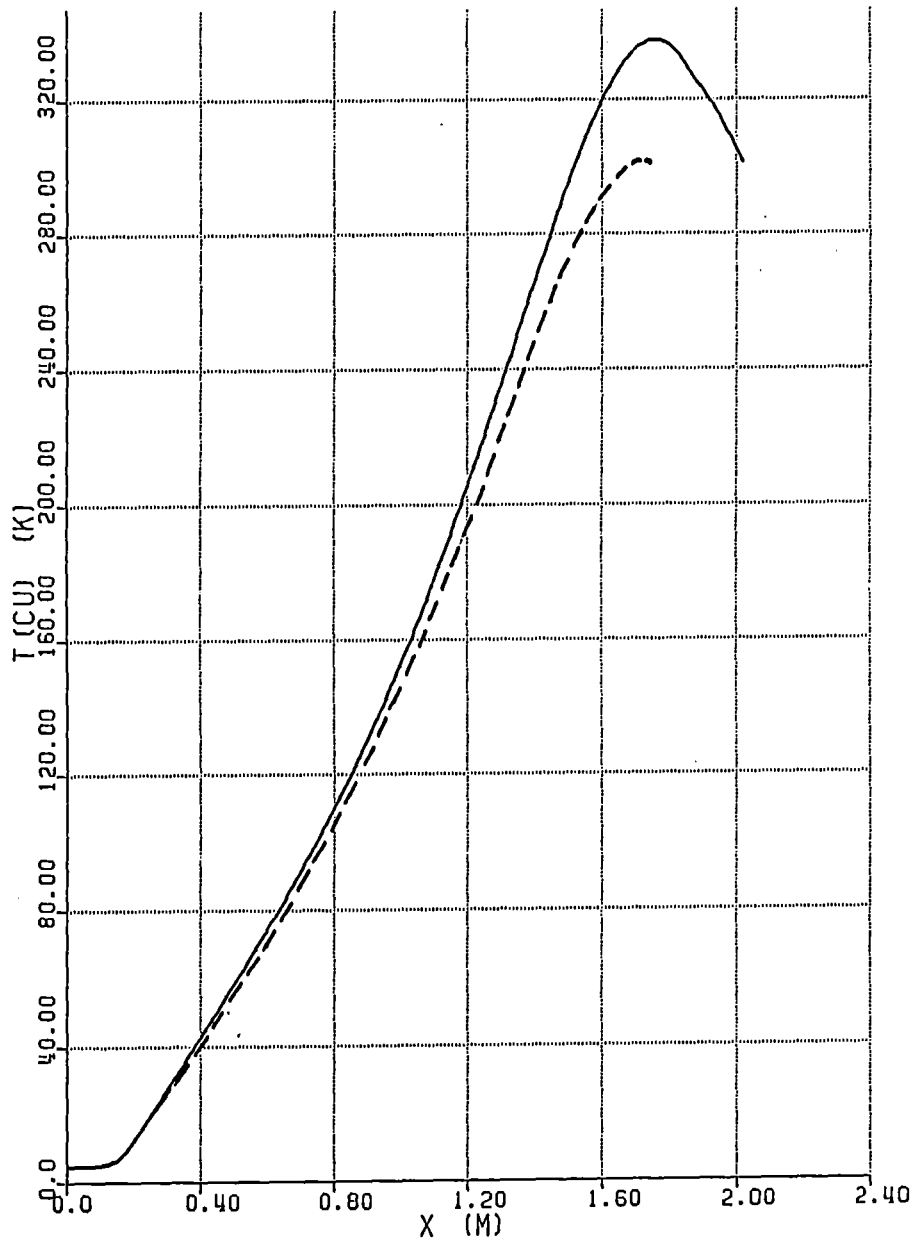
Figure 40. **Temperature distribution of the current lead:** With (full line) resp. without warm end terminal (dashed line)

Parameters	Unit	Value
I	A	23000
$\dot{m}$	$\dfrac{g}{s}$	1.42
$L_{h.e.}$	m	1.40
$L_{c.l.}$	m	1.82
p_{inlet}	bar	4.0
T_{inlet}	K	4.5
T_{outlet}	K	301.0
$\dfrac{L\,I}{A_{Cu}}$	$\dfrac{A}{m}$	$1.04\ 10^{7}$

Table 11. **Optimized parameters for the POLO current lead**

6.3 Behaviour of the optimized current lead during other running conditions:

As a result of the preceding studies the shape factor (see eq. (2.2)) has been obtained, i.e.

$$\frac{L\,I}{A} = 1.04\,10^7\,\frac{A}{m,}$$

e.g. the optimum length of the heat exchanger could be calculated now for other running conditions. It should be mentioned that L_{opt} corresponds **only** to the length of the heat exchanger and **not** to the length of the whole current lead, i.e. bottom (cold-) and top (warm-)end terminals remain fixed.

$$\frac{L_1\,I_1}{A} = \frac{L_2\,I_2}{A} = \text{const.,} \tag{6.2}$$

This results in

$$L_2 = L_1\,\frac{I_1}{I_2}. \tag{6.3}$$

The helium mass flows were scaled by the inverse ratio of currents as has been done for the lengths.

Because the cold and warm ends remain fixed in length the length of the heat exchanger has to be reduced more than expected from eq. (6.3). to get minimum heat loss at the upper end terminal.

Fig. 41 shows the temperature distributions for

- zero current,
- 17 kA,
- 23 kA, and
- 30 kA.

Tab. 12 summarizes the calculation results.

I	L	$\dot{m}$	$T_{Cu,max}$	$T_{He,max}$	ΔU	Δp	Q_{cold}	Q_{warm}
[kA]	[m]	$[\frac{g}{s}]$	[K]	[K]	[mV]	[mbar]	[W]	[W]
0	2.32	0.40	285	228	0.0	0.22	-2.53	478.8
0*	2.32	4.50	285	273	0.0	0.01	-0.03	192.5
17	2.32	1.05	301	284	94.6	1.27	-0.12	-14.5
23	1.82	1.42	304	286	102.3	1.41	-0.08	-160.2
30	1.50	1.853	315	294	114.5	1.62	-0.05	-461.2

Table 12. **Optimization for different running conditions:** * - mass flow only in the bottom part of the current lead

An interesting result has been obtained for the first condition, e.g. zero current: during the design phase it was decided to have the possibility to use a higher helium mass flow at the bottom end than for the total heat exchanger, although the calculations didn't expect that the feature will be really needed. Nevertheless for zero current condition it could be an advantage, because it comes out that only a high mass flow of 4.5 $\frac{g}{s}$ is needed at the bottom end, and no mass flow in the heat exchanger itself. The upper helium temperature is expected to be 13 K. If it will be possible to transfer the cold helium gaz to the refrigerator, then this cooling mode should be preferred, because if a mass flow is used along the whole heat exchanger the upper helium temperature at the warm end will be less than 230 K, e.g. the current lead will be frozen. A further advantage is that the superconducting part of the heat exchanger, i.e. the 15 cm long cold end, is below 16 K, e.g. the superconductors stay superconducting. Fig. 42 shows the temperature distributions for zero current and the two different cooling modes.
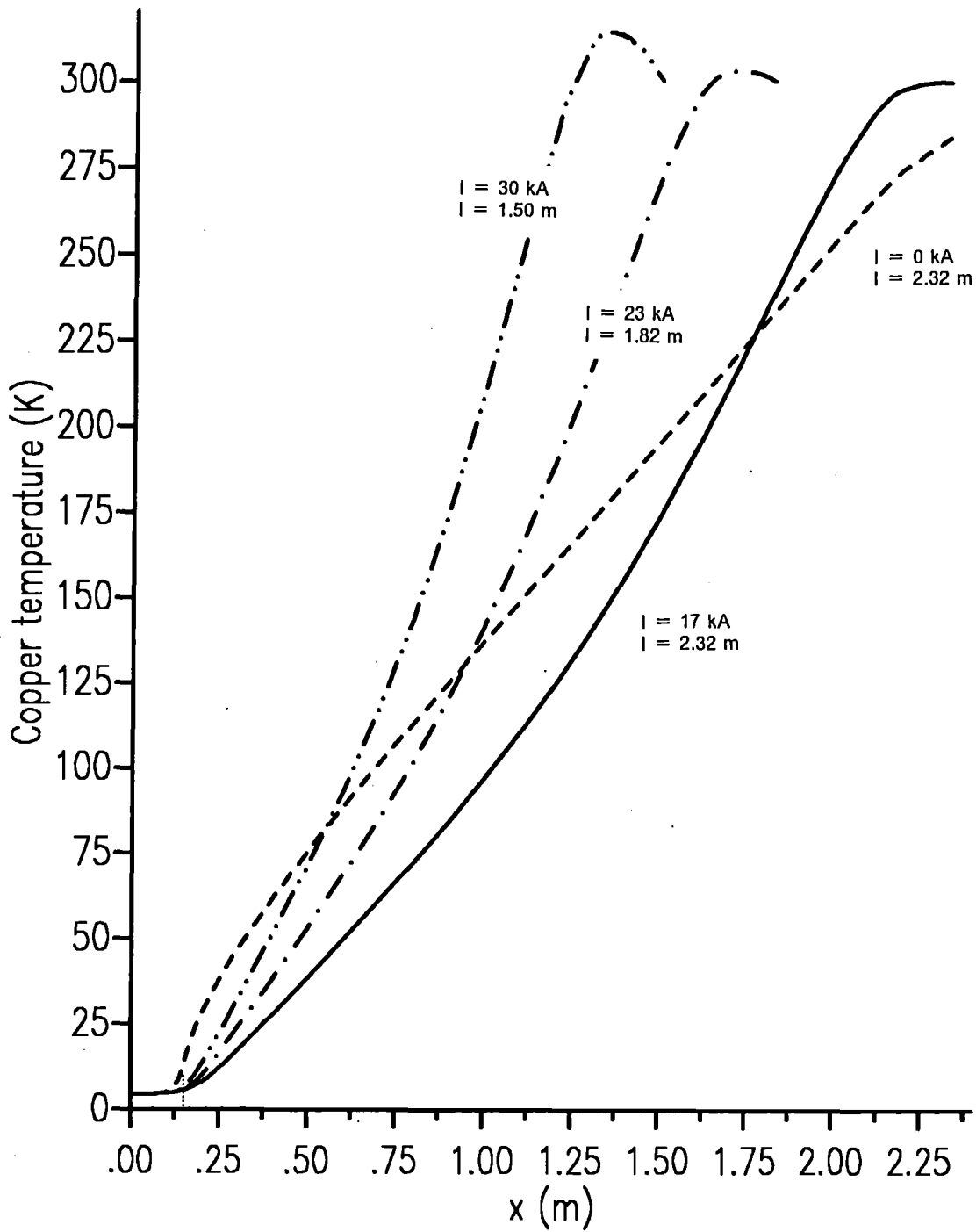
Figure 41. Temperature distribution of the current lead for different running conditions: POLO current lead
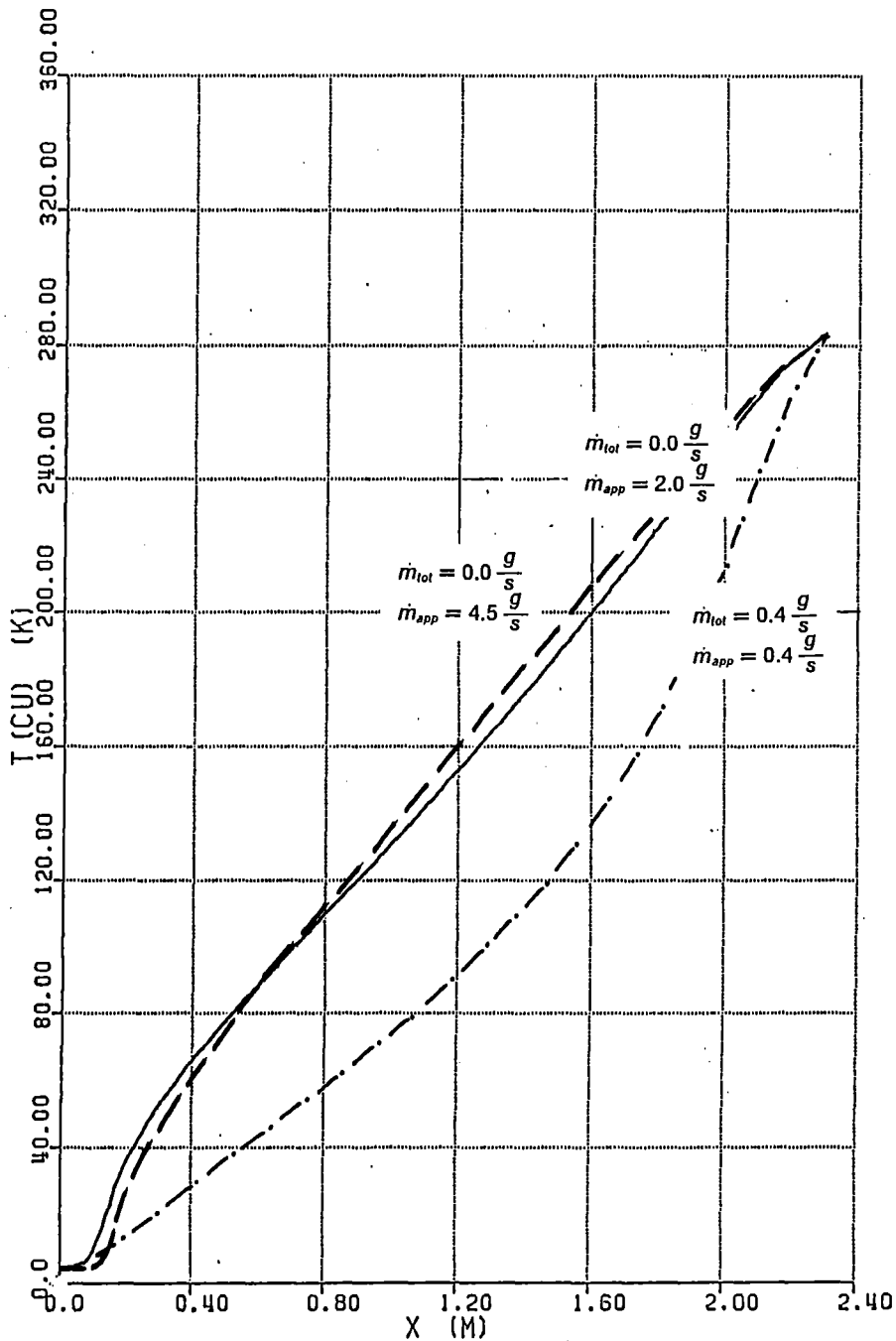
Figure 42. **Temperature distribution for zero current and different cooling modes:** POLO current lead

At the end of this chapter some emphasis will again be given to the alternative calculation using the parallel-flow model. As already shown for the TORE SUPRA current lead the friction factor ξ which enters into the pressure drop equation and represents the geometry has much lower values in case of the Dittus-Boelter type than for the cross-flow type.

For measuring the hydraulic behaviour a 530 mm long model of the POLO heat exchanger was built and measured at room temperature [31]. For historical reasons the cross section of the copper bar was larger than in case of the real current lead. Therefore the hydrodynamic properties changed slightly.

Using the helium mass flow and the inlet pressure of the test a series of calculations have been made for both models. Fig. 43 shows the friction factor ξ as a function of the Reynolds number Re. Again a significant difference have been observed. The measurement data are also shown which have been obtained by using the equations of chapter 2 to get the hydraulic diameter and the Reynolds number, and by means of the measured pressure drop the friction factor. A significant difference has been obtained, and as a conclusion it should be mentioned that the numbers obtained by means of the croos-flow model are in a good agreement, although the slope is fifferent.

In addition to this also the pressure drop as a function of the mass flow was calculated and compared with the measurements (Fig. 44 top). Both models didn't reproduce the pressure drop distribution very well. By changing the equivalent wire diameter - and as a consequence the hydraulic diameter - the calculated pressure drop follows the measured one nicely.

In contradiction to this the pressure drop distribution obtained by calculating the Nusselt number by means of the Dittus-Boelter equation didn't follow the measured values very well, especially at low helium mass flow rates (see Fig. 44 bottom). An adjustment to lower pressure drops leads to a disagreement at higher numbers.
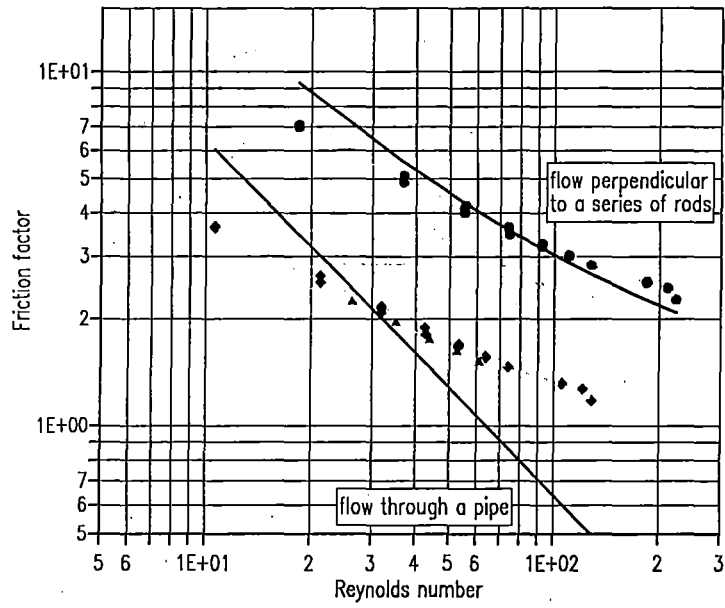
Figure 43. **Friction factor vs. Reynolds number for different models: calculation and measurement data:** POLO current lead
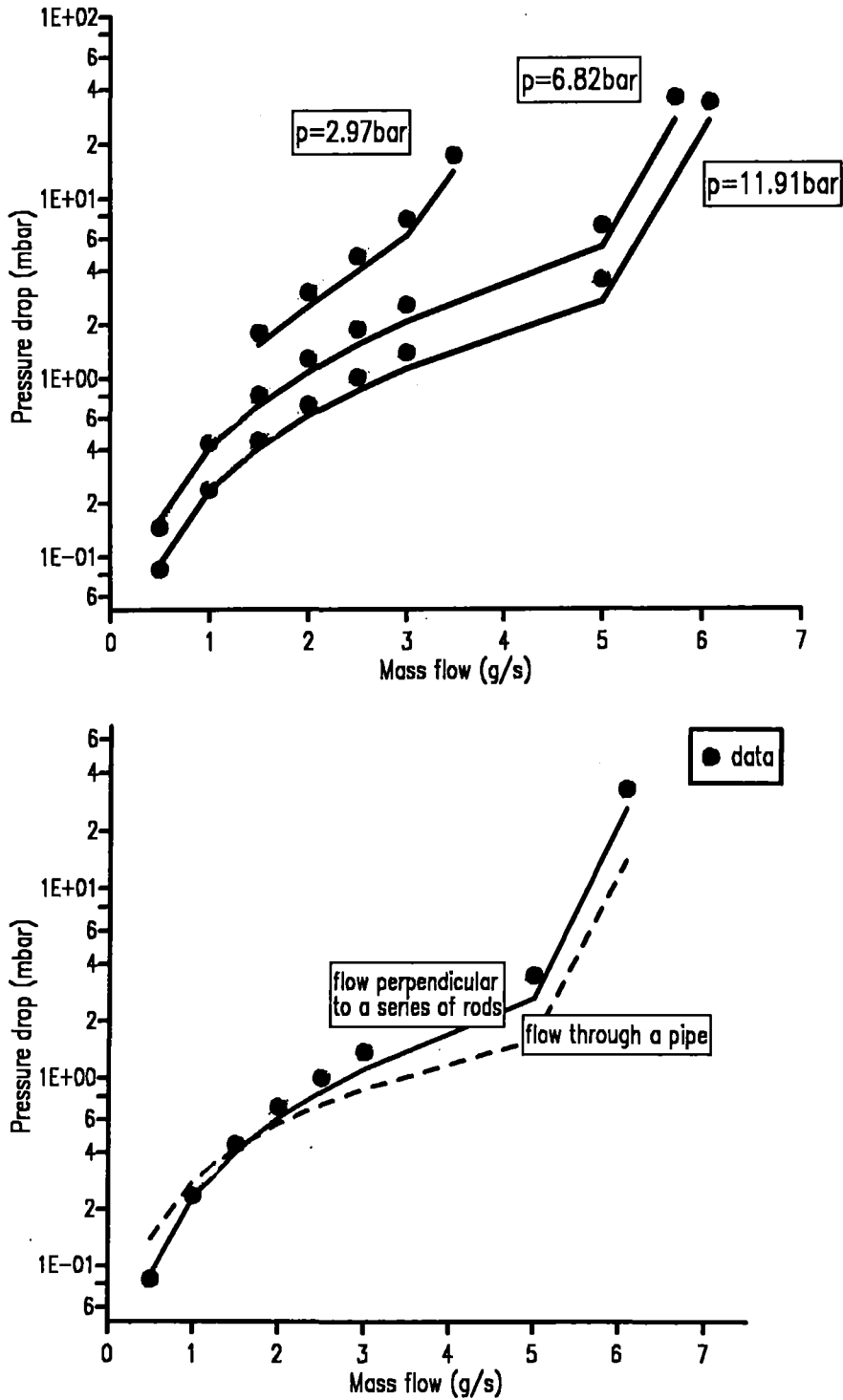
Figure 44. Calculated and measured pressure drop vs. mass flow:

top: using the model of a flow perpendicular to a series of rods (p denotes the inlet pressure)

bottom: comparison of the two models (for p_{in} = 11.91 bar)

6.4 Use of a variable length of the current lead

Due to the fact that the optimized length of a current lead is only valid for **one** current case the program CURLEAD was changed in the following way: the length of the cold end where the superconductors are put in parallel was let free, e.g. no heat production was assumed when the copper temperature was less than 10 K. This assumption approximates the fact that Nb_3Sn wires will be put in parallel to the copper bar of the heat exchanger along a length of 1.1 m [30].

The effect was studied by using the 17 kA case and varying the helium mass flow. Fig. 45 shows the results obtained with a fixed cold end of 15 cm length, while in Fig. 46 the corresponding temperature distributions are plotted for the variable cold end case. It can be seen that for small mass flows the "new" model gave a more realistic result because the 10 K point moved towards the cold end which means that there will be no more any superconducting part in the current lead. Therefore higher temperatures and higher heat losses were obtained. On the other side if the 10 K point was inside the heat exchanger the calculations using the "old" model gave the maximum temperature distribution which were possible for the given mass flow. Using a superconducting bus a sharper temperature distribution has been obtained, and the maximum copper temperature was lowered, too.

The shape of the temperature distribution, and the maximum temperature as well, will strongly depend on the helium mass flow i.e. they destabilize the lead. On the other hand the time scale for reaching a steady state condition is in the order of 10 min (see next chapter) a feedback system which will be "fast" in this scale will stabilize this effect.

The reduction of helium mass flow as calculated by means of CURLEAD is in the order of 5 to 10 percent.

The main advantage of the self-adjusting length of the heat exchanger by means of the superconducting wires is the fact that the current lead is "optimimized" between 15 and 30 kA. Smaller currents can be run by increasing the mass flow at the cold end and leaving the warm end of the heat exchanger optimized. Fig. 47 shows the temperature distributions obtained by using the self-adjusting length for different currents.
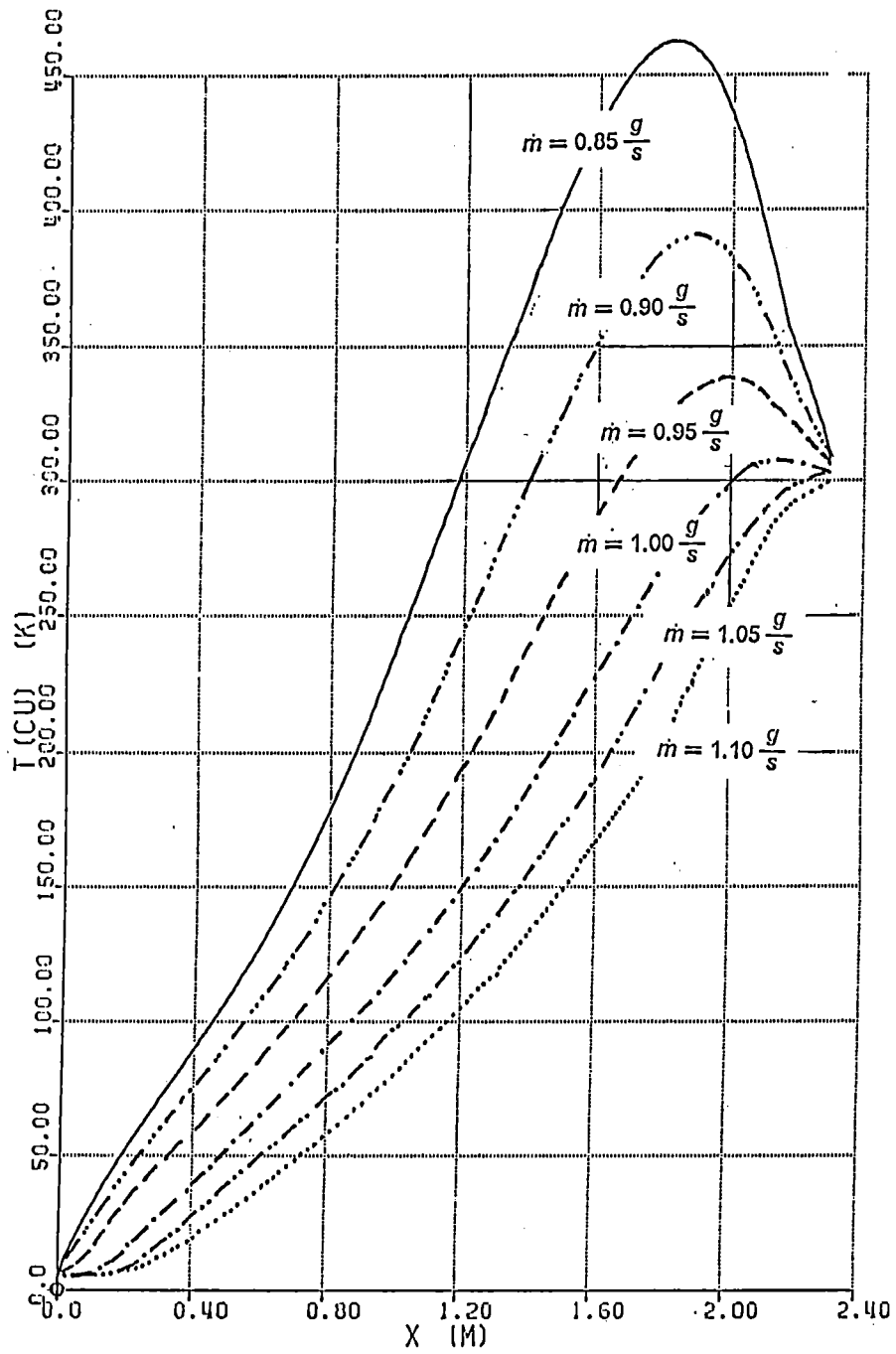
Figure 45. Temperature distribution for different helium mass flows (I = 17 kA, "old" model): POLO current lead
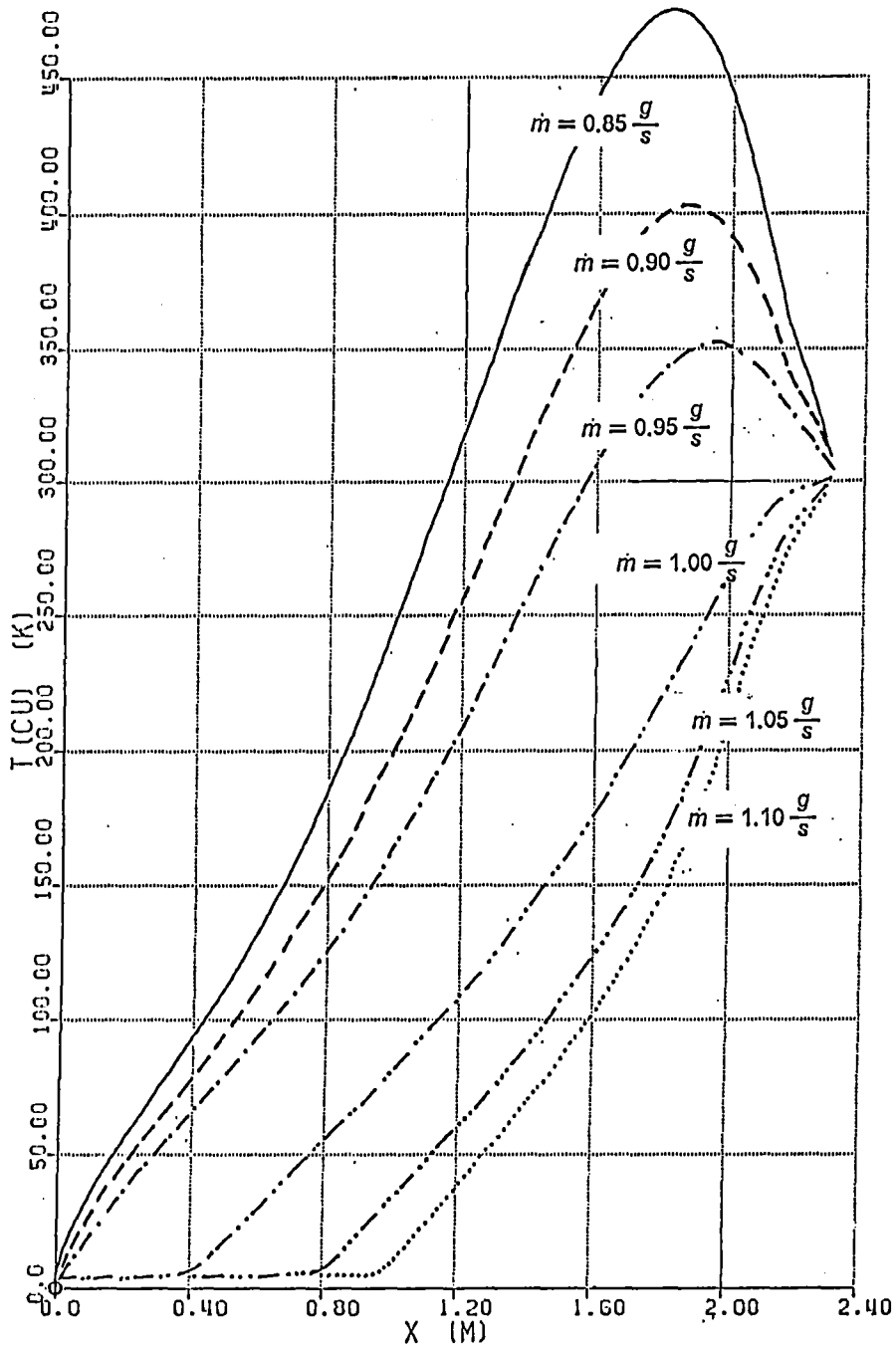
Figure 46. Temperature distribution for different helium mass flows (I = 17 kA, "new" model): POLO current lead
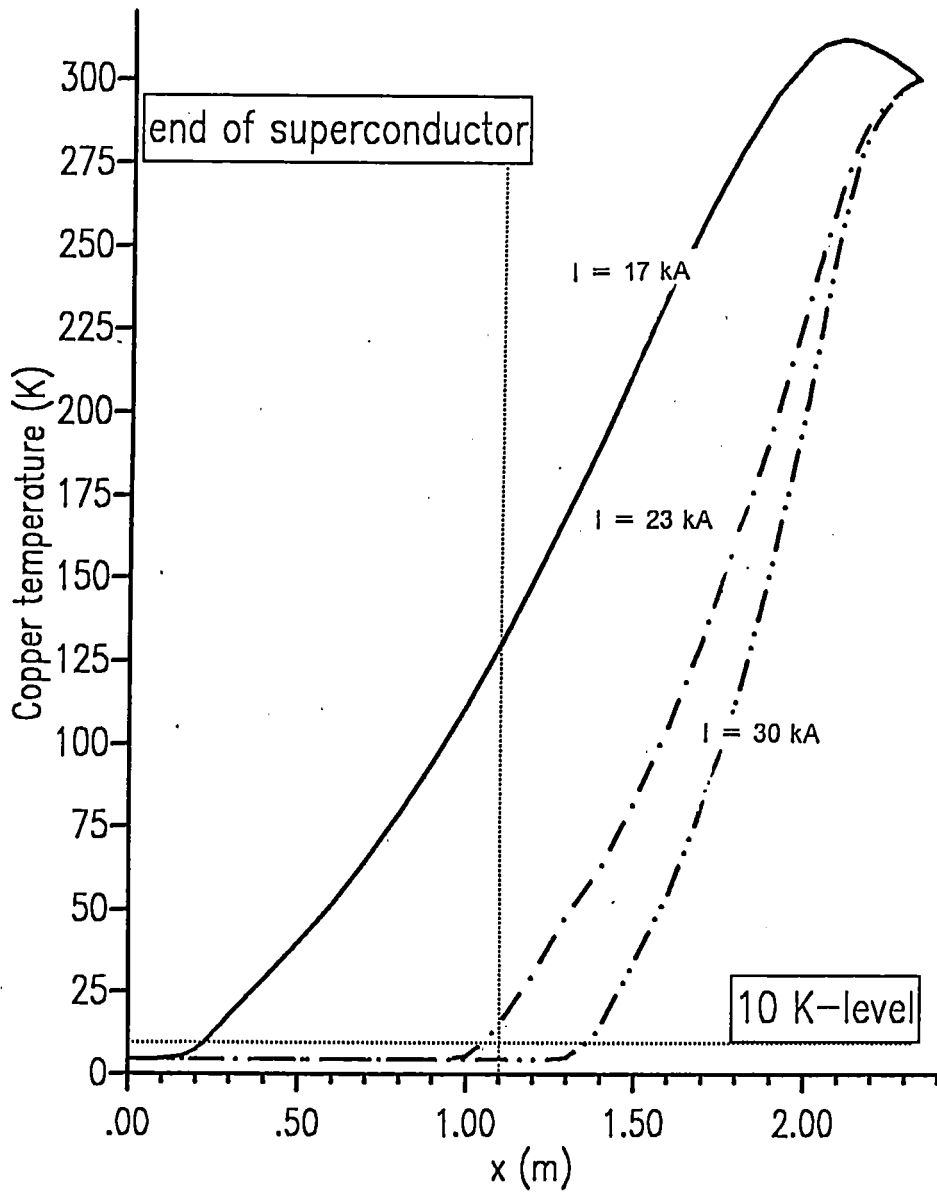
Figure 47. **Temperature distributions for different currents ("new" model):** POLO current lead

6.5 Boil-off case of the current lead

Next the transient behaviour of the POLO current lead is presented. As an example only the 17 kA case has been calculated. Because of the low conductivity copper used for the current lead the change of the maximum temperature is marginal (see for example chapter 4). Much more interest is given to the temperature slope, i.e. the heat loss, at the cold end due to the presence of the superconductors in parallel. Fig. 48 shows the temperature distributions obtained with a fixed cold end of 15 cm. The maximum temperature didn't change within 5 minutes, and after 20 minutes it rises up to 330 K.

In Fig. 49 the temperature at x = 15 cm is plotted as a function of time. It should be mentioned that the corresponding heat losses are underestimated in the sense that the superconducting part of the heat exchanger (i.e. the so called "appendix") will produce internal heat after at least 5 seconds.

6.6 Comparison to the ideal heat transfer

At the end results are presented which are obtained by using an ideal heat transfer and assuming the validity of the Wiedemann-Franz law as well (see chapter 2.1). To study the effect only the heat exchanger has been calculated (no cold and warm end terminals) by means of CURLEAD and the cooling perimeter has been reduced by a factor of two (P_{co} = 5.75 m instead of P_{co} = 11.49 m) to obtain a larger effect. The "Wilson scheme" has been simulated be replacing the heat transfer term in the heat conduction equation by the helium mass flow term, and the helium temperature was set to the heat exchanger one. Fig. 50 shows the temperature distributions obtained with both schemes.
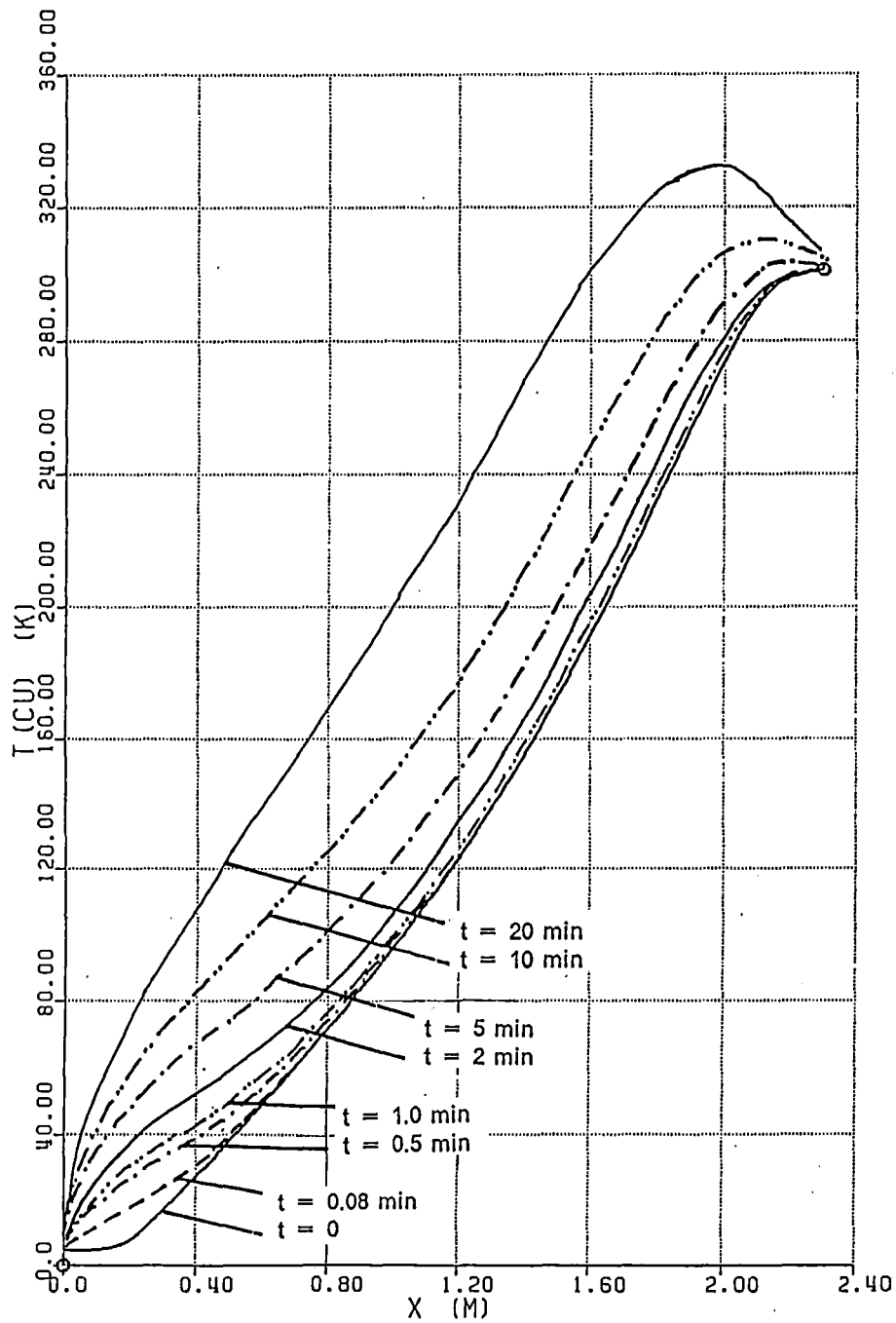
Figure 48. **Temperature distributions for different boil-off times (I = 17 kA, "old" model):** POLO current lead
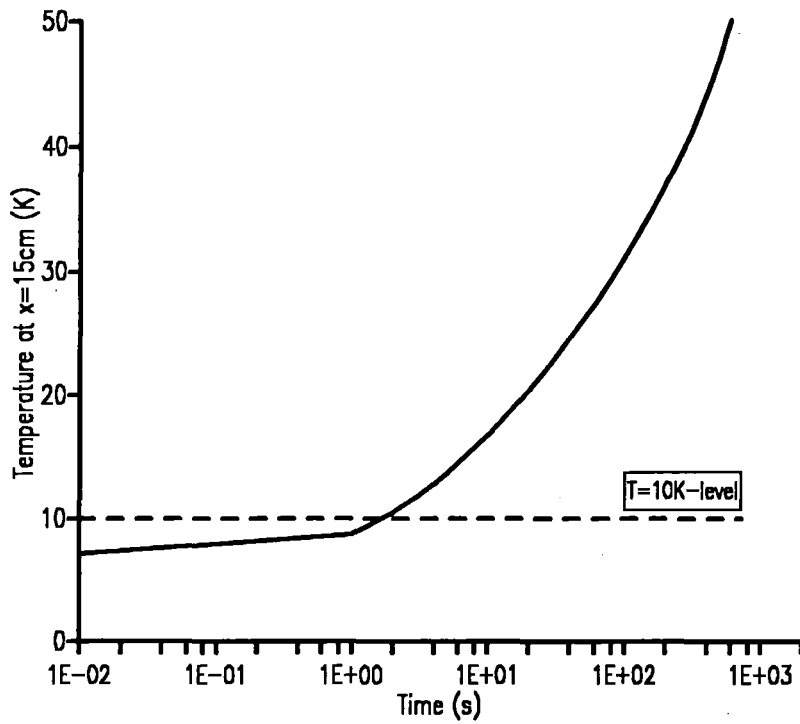
Figure 49. Temperature at x = 15 cm vs. time: POLO current lead
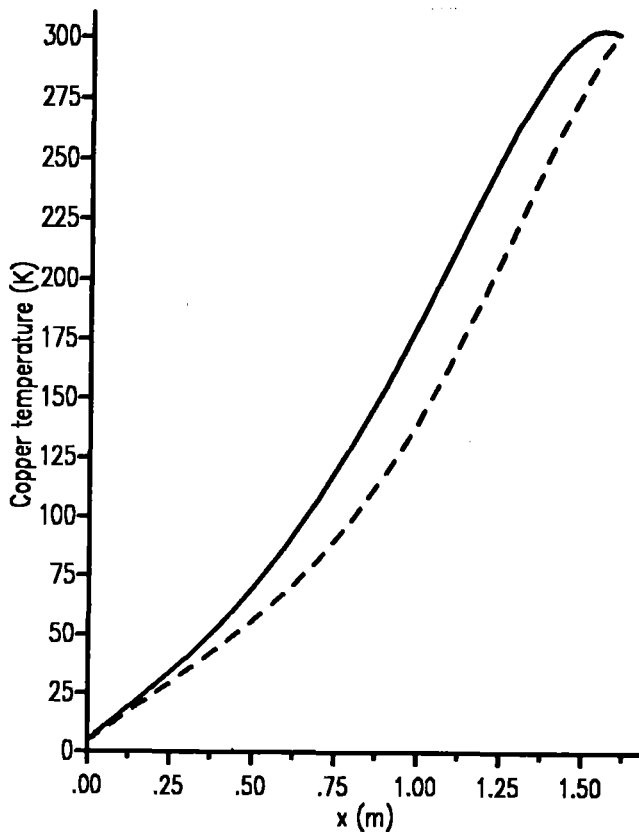
Figure 50. Temperature distribution without (solid line) and with (dashed line) ideal heat transfer: POLO current lead

As has been expected, two differences has been obtained:

- the heat loss at the cold end is smaller in case of the ideal heat transfer because no temperature difference between copper and helium has been assumed. In fact the temperature difference will be relatively large because the heat transfer will be not as good as in the warmer parts of the heat exchanger.
- The temperature gradient at the warm end of the heat exchanger is smaller in case of the ideal heat transfer. This results in a longer length as would be obtained by assuming real heat transfer.

In fact the length would be too long if ideal heat transfer would be assumed, the effect would be more drastic if the warm end terminal will be added (which is practically essentiell). This would lead to a further of the upper end temperature.

Chapter 7. Discussions and Conclusions

A computer code named CURLEAD was written solving the one-dimensional heat equation and the energy balance for the helium coolant simultaneously. The physics and the mathematical approach which enter the code have been described. The choice of variables sensitive to parameter changes has been presented and shown by means of a low conductivity copper heat exchanger. Two current leads built in the past have been recalculated.

The transient behaviour of a low and a high conductivity heat exchanger have been studied and compared with respect to stability.

The optimization study for a low conductivity current lead for the POLO model coil has been presented. Special attention was given to the forced flow mode and to the superconducting cold end appendix, too.

The importance of the knowledge of the thermal conductivity, and the electrical resistivity as well, as a function of temperature was mentioned because they are important for the optimization procedure.

The main aim of writing CURLEAD is the optimization of a current lead by taking into account the real heat transfer. This means the calculation of the heat transfer coefficient assuming physical models which describe the hydrodynamic behaviour. One model is represented by the Dittus-Boelter equation (parallel-flow model), the other one uses empiric formulas for a flow perpendicular to a series of rods (cross-flow model).

Using the temperature dependent heat transfer it has been shown that it is important to model the cold end region very carefully because the heat transfer will be small in this region and the temperature difference between the copper lead and the helium coolant will be larger than in the warmer parts of the lead.

In general the use of a temperature dependent heat transfer also leads to a shorter length of the current lead because especially at lower temperatures the heat transfer is not as good as in the warm end region. In addition it is possible to obtain a heat loss at the cold end which depends on the cooling perimeter, i.e. the heat transfer properties of the heat exchanger. If an ideal heat transfer would

be assumed the upper end will have a lower temperature which results in a longer length.

In addition the modelling of the warm end terminal which in general will be poor cooled changes the temperature distribution of the heat exchanger significantly, e.g. as has been shown for the POLO current lead. The result of the addition of the warm end terminal is a shorter length of the heat exchanger.

As has been shown for the POLO current lead, the use of superconducting wires at the cold end parallel to the copper bar is essentiell to reduce the heat generation at low temperatures. In addition it is possible to get a "self-adjusting" heat exchanger wih respect to different running conditions. The helium mass flow rate will also be reduced. This means that the current lead will be optimized between a minimum and a maximum current, I_{min} resp. I_{max}. Smaller currents can be run by increasing the helium mass flow at the cold part of the heat exchanger by leaving its warm end optimized.

Acknowledgement

This work has been performed in the frame of the European Fusion Technology Programme.

References

[1] R. Toschi," NET and the European Fusion Technology Programme", 15th Symposium on Fusion Technology, Utrecht, 19 - 23 September 1988

[2] G Brianti and K. Hubner (Eds.), "The Large-Hadron Collider in the LEP-Tunnel", CERN-87-05, (1987)

[3] B. Turck, "TORE SUPRA: a tokamak with superconducting toroidal field coils - status report after the first plasma", IEEE Trans. on Magn. Vol. 25 No. 2, (1989), 1473

[4] S. Förster, G. Friesinger, U. Jeske, H. Katheder, G. Nöther, A. Nyilas, G. Schenk, C. Schmidt, L. Siewerdt, M. Süßer, A. Ulbricht, F. Wüchner, "A 2 MJ, 150 T/s Pulsed Ring Coil. Status of the Design and the Test Arrangement", Proc. of the 9th Intern. Conference on Magnet Technology (MT-9), Zürich 9 - 13 September 1985, 32

[5] M.N. Wilson, "Superconducting Magnets", Clarendon Press, Oxford 1983

[6] J.M. Lock, "Optimization of current leads into a cryostat", Cryogenics 9, (1969), 438

[7] Touloukian et al., Thermophysical Properties of Matter, Vol. 1, New York 1970

[8] W. Bleakney et al., "Low-Temperature thermal conductivity of some commercial coppers", Journ. of Appl. Phys., Vol. 28, (1957), 1282

[9] VDI-Wärmeatlas, "Berechnungsblätter für den Wärmeübergang", Hrsg. vom Verein Deutscher Ingenieure, VDI-Verlag, Duesseldorf, 1974

[10] E. Tada et al., "Development of high-current vapor-cooled current lead for fusion", presented at the 1985 CEC, Boston, Aug. 13-16

[11] E. Tada et al., "Experience on high current leads for superconducting magnets; seven types from 1 kA to 30 kA", Cryogenics 24 (1984), 200

[12] K. Ishibashi et al., "Design chart of optimum current leads", Adv. Cryog. Eng. 31, (1986), 235

[13] K. Maehata et al., "Optimization method for superconducting magnet current leads", Cryogenics 28, (1988), 744

[14] D.R. Croft and D.G. Lilley, "Heat Transfer Calculations using Finite difference Equations", Applied science publishers ltd., London 1977

[15] D. Marsal, "Die numerische Lösung partieller Differentialgleichungen", Bibliographisches Institut, Zürich 1976

[16] R. Heller, "Description of the computer code CURLEAD for optimizing current leads for superconducting magnets", in preparation

[17] B.A. Hands, "HEPROP - a computer programme for the thermodynamic and thermophysical properties of helium", Cryogenics Laboratory, Dept. of Engineering Science, Oxford University, Department Report 1289/79 (1979)

[18] D. Leroy and L. Oberli, "18 kA vapour cooled current leads", CERN SPS/88-35 (EMA) - LHC Note 80

[19] F. Viargues, G. Claudet, J. Challier, D. Chatan, " Amenees de courant 15 000 A compte-rendu s'essais," C.E.A. - C.E.N.G., Note SBT/CT/88-09

[20] D. Güsewell and E.-U. Haebel, "Current leads for refrigerator-cooled large superconducting magnets", Proc. 3rd Int. Cryog. Eng. Conf. (ICEC 3), (1970), 187

[21] L. Oberli, private communication

[22] J. D. Ye, private communication

[23] Y. Lühning, private communication

[24] W.B. Fowler, D. Drickey, P.J. Reardon, B.P Strauss, D.F. Sutter, "The Fermilab Energy Doubler, a two-years progress report", IEEE Trans. on Nucl. Science, Vol. NS-22 No. 3, (1975), 1125

[25] R. Perin, "Progress on the superconducting magnets for the LHC", IEEE Trans. on Magn., Vol. 24 No. 2, (1987), 734

[26] S. Wolff, "Superconducting HERA magnets", IEEE Trans. on Magn., Vol. 24 No. 2, (1987), 719

[27] SSC Central Design Group, "Conceptional Design of the Superconducting Supercollider", Lawrence Berkeley Laboratory, CDG SSC-SR-2020, (1986)

[28] C.E. Taylor, "SSC Magnet Technology", IEEE Trans. on Magn., Vol. 24 No. 2, (1987), 726

[29] D.S. Beard, W. Klose, S. Shimamonto and G. Vécsey (eds.) "The IEA Large Coil Task. Development of Superconducting Torodial Field Magnets for Fusion Power", Fusion Engineering and Design, 7 (1 & 2), (1988)

[30] S. Förster, G. Friesinger, U. Jeske, G. Schenk, A. Ulbricht, to be published

[31] G. Friesinger, private communication

Appendix A. Flow chart of the computer code CURLEAD